PHILOSOPHICAL TRANSACTIONS OF THE ROYAL SOCIETY A

Phil. Trans. R. Soc. A (2008) **366**, 1231–1274
doi:10.1098/rsta.2007.2130
Published online 5 November 2007

Modelling vortex-induced fluid–structure interaction

By Haym Benaroya[1,2,*] and Rene D. Gabbai[1,2]

[1]*Department of Mechanical and Aerospace Engineering, Rutgers University, New Brunswick, NJ 08854-8058, USA*
[2]*NIST, Gaithersburg, MD 20899-1070, USA*

The principal goal of this research is developing physics-based, reduced-order, analytical models of nonlinear fluid–structure interactions associated with offshore structures. Our primary focus is to generalize the Hamilton's variational framework so that systems of flow-oscillator equations can be derived from first principles. This is an extension of earlier work that led to a single energy equation describing the fluid–structure interaction. It is demonstrated here that flow-oscillator models are a subclass of the general, physical-based framework. A flow-oscillator model is a reduced-order mechanical model, generally comprising two mechanical oscillators, one modelling the structural oscillation and the other a nonlinear oscillator representing the fluid behaviour coupled to the structural motion.

Reduced-order analytical model development continues to be carried out using a Hamilton's principle-based variational approach. This provides flexibility in the long run for generalizing the modelling paradigm to complex, three-dimensional problems with multiple degrees of freedom, although such extension is very difficult. As both experimental and analytical capabilities advance, the critical research path to developing and implementing fluid–structure interaction models entails

— formulating generalized equations of motion, as a superset of the flow-oscillator models; and
— developing experimentally derived, semi-analytical functions to describe key terms in the governing equations of motion.

The developed variational approach yields a system of governing equations. This will allow modelling of multiple d.f. systems. The extensions derived generalize the Hamilton's variational formulation for such problems. The Navier–Stokes equations are derived and coupled to the structural oscillator. This general model has been shown to be a superset of the flow-oscillator model. Based on different assumptions, one can derive a variety of flow-oscillator models.

Keywords: vortex-induced vibration; reduced-order modelling; circular cylinder; Hamilton's principle; fluid–structure interaction

1. Background

The problem of vortex shedding from bluff bodies has been examined for over a century, as reflected by the extensive literature on the subject. The focus of these foregoing research efforts can be split into two broad categories: investigations

* Author for correspondence (benaroya@rci.rutgers.edu).

One contribution of 6 to a Theme Issue 'Experimental nonlinear dynamics II. Fluids'.

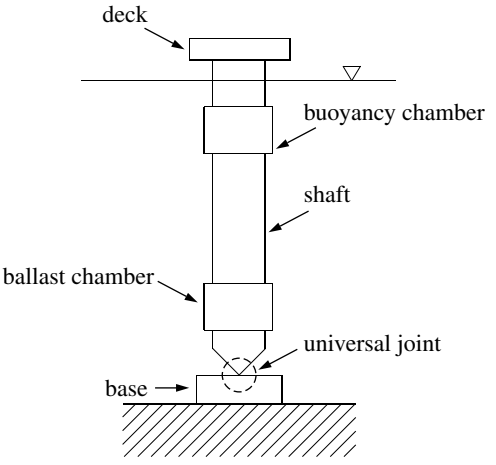

Figure 1. Schematic of a typical articulated tower.

into the flow characteristics around a bluff body in a flow and studies of the response of such bodies to the forces from the flow.

The approach sought here, to derive a set of reduced equations of motion for a structure subjected to vortex-shedding loads from first principles, represents a novel approach to a long-studied problem. Such reduced equations are generally called flow-oscillator models. The work at hand also embraces two disciplines: vortex shedding from bluff bodies, and the dynamics of a compliant offshore structure. We begin with a sampling of the literature available on both of these topics. While there is a huge literature of numerical approaches to these problems, we view them as outside the scope of this paper.

(*a*) *Compliant offshore structures*

Compliant structures provide an attractive alternative to traditional offshore platforms. Traditional platforms resist forces due to current, waves and wind. These structures are assumed to undergo displacements small enough to allow linear dynamic methods to be used to solve for the response. Compliant structures also undergo small displacements, but these displacements are large enough to necessitate the introduction of nonlinear methods to solve for the structural response. An extensive review of the nonlinear dynamics of compliant structures has been presented by Adrezin *et al.* (1996). Compliant structures are better suited than traditional frame structures for deeper water applications, since such facilities need not be as reinforced against the ocean environment as the more traditional structures.

Articulated towers, used for shallow water purposes, are attached to the ocean bottom via a universal joint, as shown in figure 1. The tower includes a ballast chamber near the base and a buoyancy chamber nearer the surface. The universal joint allows tower motion to occur in three dimensions.

The tension leg platform (TLP) design takes a different approach to surviving the ocean environment. A schematic of a typical TLP is given in figure 2. The TLP consists of a platform connected to a submerged pontoon (to provide buoyancy). The platform system is in turn moored to the ocean floor via several slender, flexible cables attached to the corners of the platform.

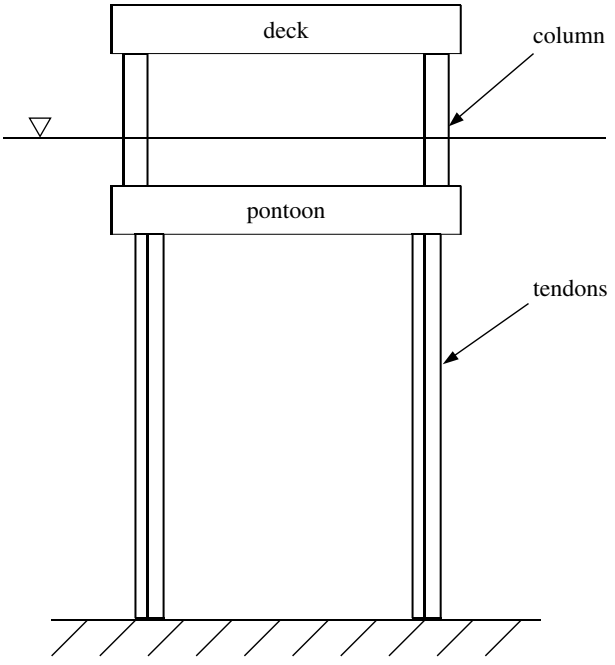

Figure 2. Schematic of a typical TLP.

Both the articulated tower and a single mooring cable of the TLP may be modelled as a partially submerged beam. The methods used here can then be used as a preliminary basis for understanding and modelling the full articulated tower or TLP.

(*b*) *Vortex-induced vibration*

The phenomenon of vortex-induced vibration has been investigated for many years. Previous reviews of the subject matter have been performed by Marris (1964), Berger & Wille (1972), King (1977) and Sarpkaya (1979). More recently, these earlier reviews have been updated by Griffin (1982), Bearman (1984) and Billah (1989). Also, Zdrakovich (1996) provides an overview of different modes of vortex shedding.

Vortex-induced vibration is based on the von Kármán vortex street. An important aspect of vortex-induced vibration is *lock-in* or *synchronization*. As the flow velocity past a responding bluff body increases, the frequency at which vortices are shed from the body increases almost linearly with flow velocity. However, when the vortex-shedding frequency reaches the natural frequency of the structure, the vortex-shedding frequency does not further increase with flow velocity. Rather, the shedding frequency remains 'locked in' to the natural frequency of the structure. At a higher flow velocity the linear dependence of shedding frequency upon flow velocity resumes (figure 3). Within the synchronization region, large body motions are observed (the structure undergoes near-resonant vibration). The lock-in phenomenon has been of great interest to many researchers, both for description of the underlying fluid dynamical mechanisms causing synchronization and for prediction of structural responses.

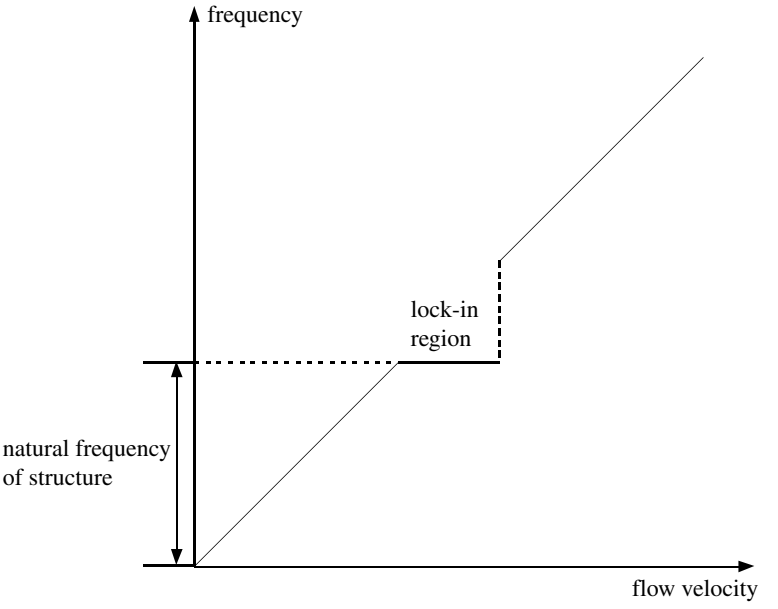

Figure 3. Plot of vortex-shedding frequency versus flow velocity.

According to Gupta *et al.* (1996), modelling approaches for structures undergoing vortex-induced vibration can be classified into three main types. The first class consists of wake–body coupled models, in which the body and wake oscillations are coupled through common terms in equations for both. The second class relies upon measurement of force coefficient data from experiments. The third class uses a single dynamic equation, but includes aeroelastic forcing terms. We do not discuss this third class in this paper.

(i) *Wake–body coupled models*

This approach seems to be the oldest and, as such, is very common. This form of modelling, according to Hartlen & Currie (1970), was introduced by Birkhoff & Zarantanello (1957). Earlier models include those developed by Bishop & Hassan (1964), Skop & Griffin (1973) and Iwan & Blevins (1974). For example, Hartlen & Currie assume a simple spring–mass–damper equation for the cylinder, dependent upon a time-varying lift coefficient. They then stipulate a second-order nonlinear differential equation for the lift coefficient, and choose the parameters in the two equations to match experimental observations. Their equations for the cylinder displacement and lift coefficient dynamics are

$$\left.\begin{aligned} x_r'' + 2\zeta x_r' + x_r &= a\omega_0^2 c_{\mathrm{L}}, \\ c_{\mathrm{L}}'' - \alpha\omega_0 c_{\mathrm{L}}' + \frac{\gamma}{\omega_0}\left(c_{\mathrm{L}}'\right)^3 + \omega_0^2 c_{\mathrm{L}} &= b x_r', \end{aligned}\right\} \tag{1.1}$$

where ω_0, a and ζ are known parameters, and α and b are parameters with values selected to best fit experimental data. Note that the second of equations (1.1) resembles a van der Pol oscillator. In actuality, it is a Rayleigh oscillator

(Jordan & Smith 1994). Both oscillators possess the desired self-excited, self-limiting behaviour observed in experiments, and thus the choice of one over the other is entirely discretionary.

Later models add further refinements to the general ideas put forth by Hartlen & Currie. Many varieties of the wake–body coupled model make use of a van der Pol oscillator for the lift coefficient (chosen owing to its inherent self-limited character as mentioned above). Investigators focusing on this method include Goswami *et al.* (1993*b*) and Skop & Balasubramanian (1995*a*,*b*). Balasubramanian & Skop (1999) reported improved results when including a stall parameter with the van der Pol oscillator. Barhoush *et al.* (1995) combined a van der Pol oscillator approach with a two-dimensional finite element mesh, resulting in a good representation of steady-state vortex-induced vibration behaviour at 'high computational cost'. Gupta *et al.* (1996) identify the important parameters for a van der Pol wake oscillator model and then solve such a model.

However, in his discussion of different types of vortex-shedding models, Billah (1989) stated that the van der Pol oscillator does not 'describe the "interaction" between "the flow and body motion" but that between "the flow and fixed body".' Billah then provides his own wake oscillator model,

$$\left.\begin{aligned} \ddot{q}_1 + 2\xi\omega_\mathrm{n}\dot{q}_1 + \omega_\mathrm{n}^2 q_1 + 2\alpha q_1 q_2 + 4\beta q_2 q_1^3 + \left(\gamma q_1 + \varepsilon q_1^3\right)\dot{q}_2^2 = 0, \\ \ddot{q}_2 + f(q_2, \dot{q}_2) + (2\omega_\mathrm{s})^2 q_2 + \alpha q_1^2 + \beta q_1^4 - 2\left(\gamma q_1 + \varepsilon q_1^3\right)\dot{q}_1 \dot{q}_2 = 0, \end{aligned}\right\} \tag{1.2}$$

where ω_n is the system natural frequency; ω_s is the vortex-shedding frequency; $f(q_2, \dot{q}_2)$ is an arbitrary function (which can itself be a van der Pol or Rayleigh equation; Billah 1989); and α, β, γ, ε are problem-specific constants. The coordinates (q_1, q_2) are the structural and wake coordinates, respectively.

Lu *et al.* (1996) apply the method of multiple scales to the wake oscillator approach, including an extra 'hidden' flow variable in the equations of motion. Their results identify several facets of the main response and the harmonics, with the method's effectiveness dependent upon the degree of fluid–structure interaction. Zhou *et al.* (1999) also use a wake oscillator approach, solving the fluid wake and the structure response in an iterative fashion.

Krenk & Nielsen (1999) develop a coupled oscillator model using an energy transfer approach to arrive at the mutual forcing terms. Their equations are

$$\left.\begin{aligned} m_0\left(\ddot{x} + 2\zeta_0\omega_0\dot{x} + \omega_0^2 x\right) &= \frac{1}{2}\rho U^2 Dl\frac{\dot{w}(t)}{U}\gamma, \\ m_\mathrm{f}\left[\ddot{w} - 2\zeta_\mathrm{f}\omega_\mathrm{s}\left(1 - \frac{w^2 + \dot{w}^2/\omega_\mathrm{s}^2}{w_0^2}\right)\dot{w} + \omega_\mathrm{s}^2 w\right] &= \frac{1}{2}\rho U^2 Dl\frac{\dot{x}(t)}{U}\gamma, \end{aligned}\right\} \tag{1.3}$$

where l is the cylinder length; D is the diameter; ρ is the fluid density; U is the flow velocity; and γ is a non-dimensional coupling parameter. The variable w represents the transverse motion of a representative fluid mass m_f. Note the quadratic form of the fluid damping coefficient. Values for the model parameters are taken from experiments and the model results display branching from below and above the lock-in region. The solution in the lock-in region is unstable, which the authors claim will lead to transition between the two modes of oscillation. However, changes in model parameters do not show similar effects to changes in experimental parameters.

This model is subsequently used to demonstrate the technique developed in this paper.

(ii) *Experimental force coefficient methods*

Models of this class generally make use of a single d.f. model for the structure, with force coefficients chosen to match experimental data. Kim & Lee (1990) developed a model for a vertical riser subject to a tension at the top end, obtaining results that are 'sensitive to the variation of C_d, C_m values' (drag and mass or inertia coefficients).

Chen *et al.* (1995) applied unsteady flow theory to find the fluid stiffness and damping coefficients for a cylinder in water, and then used these coefficients to construct a lift coefficient term in a single d.f. oscillator. The addition of fluid damping allowed 'negative damping'[1] to occur, allowing for high-amplitude oscillations around the lock-in region.

Cai & Chen (1996) applied a similar approach to chimney stacks in air supported by guy-lines. Their results for r.m.s. displacement of the tower agree with experimental observations. They also identified parameters that contribute to the resonant behaviour of the stack–cable system, and suggested ways to remove these resonances.

Jadic *et al.* (1998) used a time-marching technique to evaluate the fatigue life of a structure subjected to vortex-induced vibration in air. Their structure is modelled as an aerofoil, using lift, pressure and moment coefficients from the literature. The results were in good agreement with previous work on aerofoils.

Christensen & Roberts (1998) also examined an elastic cylinder in air, estimating the flow parameters recursively. Two possible models are presented in the work, one of which is more complex due to inclusion of the time dependence of wind fluctuation. The models give similar fits to experimental data, suggesting that the time dependence of wind fluctuation is not a major factor in the response.

(iii) *Experimental data and fluid dynamics*

All three classes of models above rely upon experimental results, both for data to choose proper parameters and to act as a basis for comparison for flow-oscillator solutions. The following studies concern themselves with measurement of fluid parameters, measurement of structural response or description of the fluid dynamics of the wake.

Sibetheros *et al.* (1994) examined the dynamics of the wake behind an oscillating cylinder. Their experimental set-up allowed for uniform, harmonic and biharmonic flows to be studied. Their data include velocity profiles for wakes under the various flow conditions. The results are corroborated with flow visualizations performed by Ventre (1993).

Goswami *et al.* (1993*a*) performed data collection in hopes of constructing a new vortex-shedding model. They found that the feedback from wake to body is 'an averaged phenomenon insensitive' to variations in cylinder oscillations and wake velocity in the synchronization region. They also observed, but were unable to consistently reproduce, coupling of the body oscillation to the wake oscillation.

[1] The fluid adds energy to the system, instead of the more usual reverse situation.

Recall that classical lock-in is the coupling of the wake oscillation, via shedding of vortices, to the body oscillation. The phenomenon observed by Goswami *et al.* (1993*a*) is termed 'alternate synchronization'.

Sarpkaya (1995) examined the transverse motion of oscillating cylinders restrained in the in-line direction. His conclusions support the use of averaged force coefficients to predict the onset of lock-in. These predictions are not extended to bodies allowed to oscillate in two directions (biharmonic response), nor are they extended to critical flows (flows whose Reynolds number is high enough to introduce turbulence; Fox & McDonald 1992).

Hover *et al.* (1997) examined vortex-induced effects on a towed cylinder. They used force feedback and online numerical simulation to mimic the vortex-induced vibration of marine cables. The data correlate with previous experiments in lift coefficient, phase and peak amplitude. The dynamic response spectra are found to vary between the single- and multi-mode cases of vibration. The authors attribute this effect to the existence of multiple wake interaction mechanisms for a structure with multiple vibration modes.

Nakagawa *et al.* (1998) tested circular cylinders in air at several yaw angles. Flow velocities and forces were computed by applying the cosine law for yawed cylinders, meaning the cross-flow velocity component for a cylinder at yaw angle θ, $U\cos\theta$, was used for force calculations instead of the free-stream velocity U. The cosine law was found to hold up to approximately $\theta = 45^\circ$ by correlating yawed cylinder data to findings made for unyawed cylinders by other investigators.

The types of vortices shed by cylinders are not limited to the von Kármán vortices as discussed above. Kitigawa *et al.* (1999) examined end-cell vortices, especially the effects of different cylinder end conditions on end-cell-induced vibration. Their experiments in air confirmed the existence of end-cell-induced vibration, with an onset at wind speeds three times higher than that of vortex-induced vibration. Also, the amplitude of end-cell-induced vibration was unstable, unlike the stable amplitudes encountered in vortex-induced vibration. End-cell-induced response was found to vary with varying diameter of a disc placed on the free end of the experimental cylinder.

Lin & Rockwell (1999) ran experiments on a fully submerged cylinder. Their cylinder was oriented so that its axis was parallel to the free surface, and they focused on the effects of distance between the top of the body and the free surface on vortex formation. Several fundamental aspects of vortex formation are found to depend on the gap between the cylinder and free surface.

Christensen & Ditlevsen (1999) performed experiments on elastic cylinders in a wind tunnel. They simulated natural wind turbulence by randomly varying the propeller rotation speed. The result is a stochastic lock-in profile, with the lower and upper limits of the lock-in region having normal distributions. The authors suggest methods for estimating the damage to the structure by employing Miner's rule.

2. Hamilton's principle revisited

This work follows that of McIver (1973) and Benaroya & Wei (2000). It is an extension of variational mechanics. See Benaroya & Wei (2000) for many of the details.

(a) The classical theory

From d'Alembert's principle for a system of n particles,

$$\sum_{i=1}^{n}\left(m_i\frac{\mathrm{d}^2\boldsymbol{r}_i}{\mathrm{d}t^2}+\frac{\partial \Pi}{\partial \boldsymbol{r}_i}-\boldsymbol{F}_i\right)\cdot\delta\boldsymbol{r}_i=0, \tag{2.1}$$

where $\Pi=\Pi(\boldsymbol{r}_1,\boldsymbol{r}_2,\ldots,\boldsymbol{r}_n)$ is the potential energy of the particles; $\boldsymbol{F}_i$ denotes forces without potentials acting on the ith particle; $\boldsymbol{r}_i$ is the position vector of the particle of mass m_i; and $\delta\boldsymbol{r}_i$ is a virtual displacement. The notation δ implies a variation in a function. It is an imaginary alternate configuration that complies with the system constraints. The variation equals zero where the system is prescribed. For example, at a fixed boundary or support, the variation is zero since there cannot be any work done in this case. Also, if the configuration is prescribed, then the variation equals zero because otherwise there would result a configuration that is not possible. Considering each term in equation (2.1), we note that

$$\delta\Pi=\sum_{i=1}^{n}\left(\frac{\partial \Pi}{\partial \boldsymbol{r}_i}\right)\cdot\delta\boldsymbol{r}_i \tag{2.2}$$

and

$$\delta W=\sum_{i=1}^{n}(\boldsymbol{F}_i)\cdot\delta\boldsymbol{r}_i. \tag{2.3}$$

With a few straightforward steps, d'Alembert's principle becomes

$$\delta\mathcal{L}+\delta W-\frac{\mathrm{d}}{\mathrm{d}t}\left[\sum_{i=1}^{n}\left(m_i\frac{\mathrm{d}\boldsymbol{r}_i}{\mathrm{d}t}\right)\cdot\delta\boldsymbol{r}_i\right]=0, \tag{2.4}$$

where $\mathcal{L}=T-\Pi$ is the Lagrangian of the system and T is the kinetic energy of the particles. Equation (2.4) for a discrete system may be written for a continuous system as

$$\delta\mathcal{L}+\delta W-\frac{\mathrm{d}}{\mathrm{d}t}\left[\int_v(\rho\boldsymbol{U})\cdot\delta\boldsymbol{r}\,\mathrm{d}v\right]=0, \tag{2.5}$$

where ρ denotes the density; $\boldsymbol{U}=\mathrm{d}\boldsymbol{r}/\mathrm{d}t$, the velocity field of the system at time t; $\mathcal{L}$ is the Lagrangian of the continuous system; and δW is the virtual work performed on the system by the generalized (non-conservative) forces undergoing virtual displacements. v denotes a fixed material system enclosed in a volume, over which the integration is performed.

Hamilton's principle is obtained by integrating equation (2.5) (or equation (2.4)) with respect to time over an interval t_1 to t_2, yielding

$$\delta\int_{t_1}^{t_2}\mathcal{L}\,\mathrm{d}t+\int_{t_1}^{t_2}\delta W\,\mathrm{d}t-\left[\int_v(\rho\boldsymbol{U})\cdot\delta\boldsymbol{r}\,\mathrm{d}v\right]_{t_1}^{t_2}=0. \tag{2.6}$$

If one imposes the requirement that at times t_1 and t_2 the configuration is prescribed, then it must be that $\delta\boldsymbol{r}=0$, and then the last term in the above

equation drops out, leaving only

$$\delta \int_{t_1}^{t_2} \mathcal{L}\, \mathrm{d}t + \int_{t_1}^{t_2} \delta W\, \mathrm{d}t = 0. \tag{2.7}$$

The equations of motion and their respective boundary conditions are a result of performing the stated variations.

In this case, where the configuration is prescribed at the end times, Hamilton's principle states that there is an optimal (minimum) path in time for the configuration of the system. This is not generally the case when the end times are not prescribed. It is important to emphasize the physical meaning of prescribing the configuration and how this leads to a variational principle to which there is an optimal configuration in dynamic space. Prescribing the variation $\boldsymbol{\delta r}$ at the end times implies that the system configuration is known at those times, thus leading to $\boldsymbol{\delta r}=\mathbf{0}$ and it is therefore possible to meaningfully speak of an optimal path between the end times.

3. McIver's extension of Hamilton's principle

In 1973, McIver (1973) published a work with broad implications for modelling complex fluid–structure interactions. The central feature of his work was the broadening of Hamilton's principle to include integral control volume concepts from fluid mechanics. The strength of McIver's work was in identifying an approach for analysing complex interactions where the system boundaries are not necessarily well defined or where the system configuration at two distinct times may not be readily prescribed. In the classical Hamilton's principle approach, the system contains one or more solid objects whose positions may be prescribed at specific times. That is, the system is of fixed mass containing the same material elements at all times.

By introducing Reynolds transport theorem, McIver generalized the analysis to include control volumes where the material is permitted to cross the boundaries.

McIver's system is composed of one control volume, of which one part is open and the rest is closed. Therefore, both are treated simultaneously, as shown in the two examples developed in his paper. The first is the derivation of the equation of motion of a rocket where the open part of the control surface coincides with the exhaust for combusted fuel. The second example discusses an early controversy regarding the modelling of the dynamics of a moving beam.

4. The extension to external viscous flows

McIver derived his extension for applications where the fluid is encased in the structure, and where the flow is assumed to be steady and frictionless. The equations derived above assume a steady frictionless flow. We are interested in generalizing the McIver extension of Hamilton's principle so that we can model the vortex-induced oscillation of a structure. This is a viscous external fluid–structure interaction problem. McIver's extension uses the control volume concept to account for fluid mass that enters and leaves the structure. This same idea can be applied to a control volume around a fluid that envelopes a structure.

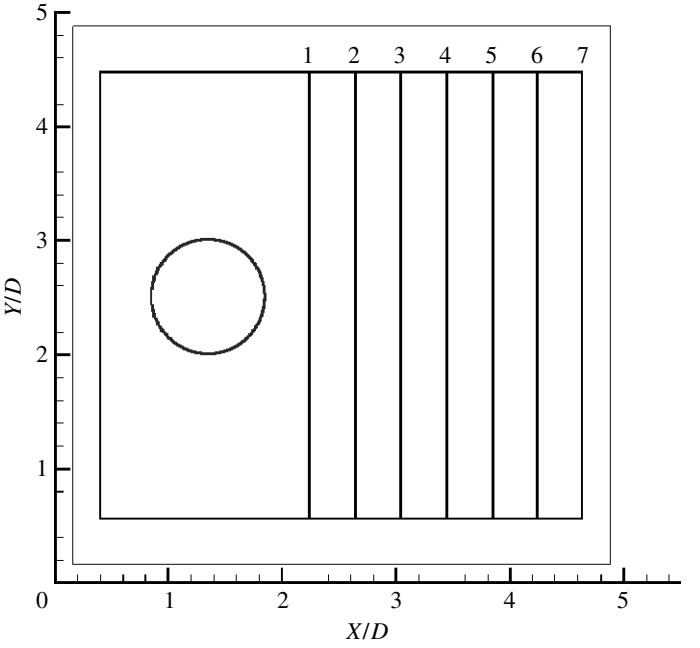

Figure 4. Top view of cylinder in a variety of possible control volumes.

Modelling of the internal flow problem has the advantage that, assuming no cavitation, the fluid is bound by the structure. With external flows, the fluid is unbounded and the modelling becomes more challenging. Full details are provided in Benaroya & Wei (2000).

In this development, it is useful to think of the system, comprising a structure surrounded by a moving fluid, as one that is defined using *two* control surfaces. The first control surface is at the structure surface. It is a closed control volume. The second control surface is at some distance from the structure, as shown in the figure 4 and figures 8–10. This control surface may be partially closed and partially open, or all open, depending on the application. It is important to keep track of the various portions of the control surface so that the parameters are appropriately prescribed.

For such a control volume, there is

— a time rate change of momentum within the control volume due to the unsteady character of the flow;
— a net momentum flux across the boundaries of the outer control surface;
— an instantaneous pressure p acting on the control surfaces; and
— an instantaneous shear stress τ acting on the control surfaces.

(*a*) *Stationary outer control volume: cylinder oscillating about contact at base*

This example is taken from Benaroya & Wei (2000). Here we take the cylinder to be connected only at its base via a leaf spring (figure 5). It behaves like a column supported only at its base. For purposes of this example we assume that the cylinder is rigid, as above, and that three-dimensional effects can be ignored.

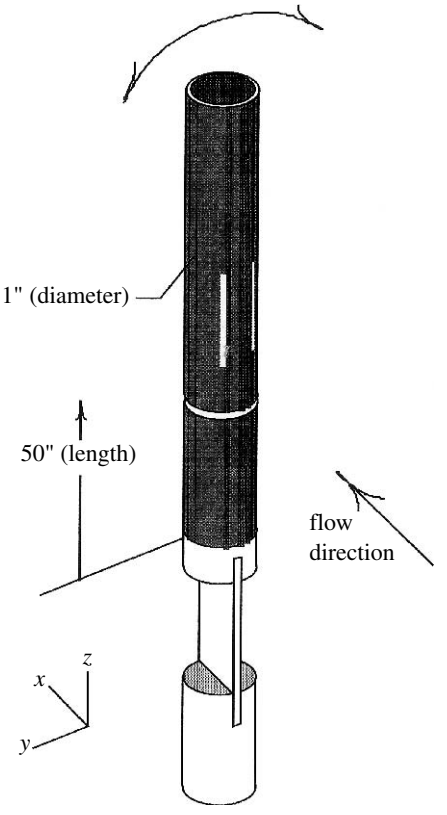

Figure 5. Schematic of test apparatus. Dimensions are in inches (1 in. = 2.54 cm).

A top view of the cylinder is shown in figure 4. There are a number of possible control volumes. Here we use control volume 4, which extends from $0.4X/D$ from the left edge of the cylinder to $1.6X/D$ from the right edge of the cylinder. This control volume appeared to capture the essential dynamics.

The single generalized coordinate that defines the cylinder location is the angle of rotation θ rad. We have an additional term in the potential of the structure due to the difference between the buoyancy force and the weight. We assume that the resultants of these distributed forces act at the geometric centre of the circular cylinder. Then, for some rotation θ, this additional potential results in the moment $(mg-B)(L/2)\sin\theta$, where mg is the weight of the cylinder; B is the total buoyancy force (which equals the weight of the displaced fluid); and L is the length of the cylinder. Let I_0 be the mass moment of inertia for the circular cylinder about its base and k_{T} be the torsional spring constant at the base. The governing equation is then

$$\dot{\theta}\left(I_0\ddot{\theta} + k_{\mathrm{T}}\theta - (mg-B)\frac{L}{2}\sin\theta\right) + m_{\mathrm{fluid}}\,U\dot{U}$$

$$= \int_{\substack{\text{closed}\\ \text{CS}}} (-p\boldsymbol{n} + \boldsymbol{\tau}_{\mathrm{c}})\cdot\boldsymbol{U}\,\mathrm{d}s + \int_{\substack{\text{open}\\ \text{CS}}} \left[-\frac{\rho}{2}U^2\,\boldsymbol{U}\cdot\boldsymbol{n} + (-p\boldsymbol{n} + \boldsymbol{\tau}_0)\cdot\boldsymbol{U}\right]\mathrm{d}s. \qquad (4.1)$$

This equation can also be evaluated numerically if written in the form

$$\frac{1}{2}\frac{\mathrm{d}}{\mathrm{d}t}\left\{I_0\dot{\theta}^2 + k_\mathrm{T}\theta^2 + (mg - B)L\cos\theta\right\} = F(t), \tag{4.2}$$

where $F(t)$ is the sum of all the remaining terms,

$$F(t) = -m_\mathrm{fluid}\,U\dot{U} + \int_{\substack{\text{closed}\\ \text{CS}}} (-p\boldsymbol{n} + \boldsymbol{\tau}_\mathrm{c})\cdot\boldsymbol{U}\,\mathrm{d}s + \int_{\substack{\text{open}\\ \text{CS}}} \left[-\frac{\rho}{2}U^2\,\boldsymbol{U}\cdot\boldsymbol{n} + (-p\boldsymbol{n} + \boldsymbol{\tau}_0)\cdot\boldsymbol{U}\right]\mathrm{d}s.$$

Then, we solve for θ by first integrating both sides of equation (4.2), and then integrating again, each integration being with respect to time. There are numerical issues to be resolved due to the complexities of the functions on both sides of the equals sign. A model problem is presented subsequently along with a brief discussion on the experimental apparatus used and the kinds of data that are obtained.

5. The initial model problem

A key objective of the present work is to prove the concept of integrating detailed experiments with reduced-order analytical modelling. In this context, we chose a geometrically simple model problem in which the fluid–structure interactions were fully coupled. That is, flow-excited structural motions that, in turn, modulated the flow. Mathematical or experimental complexities like strong three-dimensionality were deferred for future development.

The model problem addressed in this study was the vortex-induced motion of a low mass-ratio circular cylinder. The cylinder was restrained at its bottom end by a leaf spring with freedom to move in the cross-stream plane only. A schematic of this model problem is shown in figure 5. One can think of it as an inverted pendulum excited by its own periodic vortex shedding. The amplitude of motion of the free, upper end was sufficiently small that the flow could be considered to be nominally two-dimensional.

The physical model used in this study was a 2.54 cm diameter (D) cylinder constructed of thin wall aluminium tube. It was 128 cm long (L) and immersed in a uniform flow of water, approximately 107 cm deep. Therefore, the top end of the cylinder protruded through the free surface. The mass ratio $m_\mathrm{cylinder}/\rho D^2 L$ was 1.53 (m_cylinder=mass of cylinder), the damping ratio ζ was 0.054, and the cylinder natural frequency in air, thus, without added mass, was f_n=1.25 Hz. For a detailed description of the cylinder and preliminary observations of the associated flow dynamics, the reader is referred to Atsavapranee *et al.* (1999).

(*a*) *Experimental data as analytical modelling input*

This section describes the experimental methodology used to acquire key modelling data, i.e. the kinetic energy transport and work by viscous forces across the boundaries of an integral control volume. There is also a presentation of preliminary data and their application to a prototype model.

Solutions will be time-dependent expressions for the structure's motion as functions of both time and position along the structure. Attaining scientifically rigorous solutions, in turn, requires spatially and temporally resolved descriptions of the fluid 'forcing' functions on the r.h.s. as well as the fluid kinetic energy derivative on the left. Unfortunately, there is, as yet, no known generalized analytic solution to the fluid equations which could be integrated to obtain the necessary forcing functions. This tends to be a universal problem faced by modellers once the governing equations of motion have been derived.

When considering how to proceed, one immediately recognizes the risk of making assumptions without a clear understanding of the flow–structure interactions over the entire range of conditions being modelled. No matter how physically reasonable, there is a significant risk of introducing empiricism into the final solution. Without additional guidance, we would also lack the insight and confidence to realistically assess the versatility of the model.

Recent advances in video-based flow measurement techniques have enabled accurate measurement of derivative flow quantities in highly complex, turbulent flows. In particular, Shah *et al.* (1999, 2000) have used highly resolved digital particle image velocimetry (DPIV) data to compute terms in the vorticity transport equation, along with turbulent strain rates in a turbulent tip vortex shed from a half Δ-wing. Hsu *et al.* (2000) presented turbulent kinetic energy transport quantities obtained from DPIV measurements in a turbulent boundary layer.

We look to capitalize on the power of DPIV and apply it to the modelling problem outlined above. Specifically, we show how high-resolution DPIV can be used to measure fluid energy transport terms and use that information as input to a reduced-order analytical fluid–structure interaction model. We also use experiments as a validation of the model output because the structure's position is inherently part of the acquired experimental data.

The dataset consisted of an ensemble of 50 sets of 225 consecutive DPIV velocity field measurements taken at 100 ms intervals, or 1/12 of a cylinder oscillation period, in a horizontal plane perpendicular to the axis of symmetry of the cylinder at rest. The location of the measurement plane was approximately 70 cm above the floor of the test section, coinciding with the location of the amplitude measurements. The spacing between vectors was 0.19 cm corresponding to $\lambda/D=0.074$. The total duration of the sample was 22.5 s or approximately 17 cylinder oscillation periods.

It is critical to note at the outset that DPIV is 'only' a two-dimensional velocity field measurement technique. While information about pressure variations and contributions from three dimensionalities in the flow are not yet accessible, we demonstrate in this paper the power of integrating focused experiments with the analytics into a new modelling paradigm. Therefore, it is important that the DPIV method is truly two-dimensional since that is the level of detail in the analytical model.

Much detail on the experimental methodology and the details of the experimental set-up are given by Dong *et al.* (2004).

(*b*) *Flow facility*

Experiments were conducted in the free surface water channel facility at Rutgers University. Details of the flow facility may be found in Smith (1992) and

Grega *et al.* (1995). The test section measured 58.4 cm in width $\times$128 cm in depth $\times$610 cm in length. It was constructed entirely from 1.91 cm thick glass panels placed in a welded steel I-beam frame. Flow was driven by two pumps operating in parallel. Variable speed controllers were used to set the flow rate between 760 and 15 000 l m^{-1}. With the test section completely filled, the maximum flow rate corresponded to a mean free-stream velocity of approximately 30 cm s^{-1}. Free-stream turbulence levels were less than 0.1% of the mean free-stream velocity and the flow was uniform across the cross section to within 2%.

(*c*) *Applying experiments to the reduced-order analytical model*

The flow measurements from an inverted oscillating pendulum experiment were analysed and a set of time traces were developed of three key fluid kinetic energy transport terms, net kinetic energy flux, time rate of change of fluid kinetic energy, and rate of work done by viscous forces. The Reynolds number of the flow was $Re=3800$, corresponding to a reduced velocity $U^*=Uf_{\mathrm{n}}D=4.8$. At this value of U^*, there is a high degree of synchronization between the vortex shedding and the cylinder motion. The plots shown in figure 6 are precisely the fluid 'forcing' functions needed to analytically determine the motion of the cylinder. In this section, we show how these data were applied to the governing equation and compare the theoretical prediction of cylinder motion with the actual, experimentally measured oscillations.

The precise form of the equation of motion used in this analysis is equation (4.1). The equation was simulated using MATLAB in which the fluid forcing terms, appearing on the r.h.s., were the experimentally determined functions presented in figure 6. The traces are labelled as follows: $\mathrm{d}(KE)_{\mathrm{fluid}}/\mathrm{d}t$=time rate of change of fluid kinetic energy in the control volume; $(KE)_{\mathrm{fluid}}$ flux=kinetic energy flux across control surface; *viscous work*=rate of work done by viscous forces; $\mathrm{d}(KE+PE)_{\mathrm{cylinder}}/\mathrm{d}t$=time rate of change of cylinder kinetic plus potential energies; and *pressure work*=rate of work done by pressure forces, as computed from the total energy. The system includes the interior structure and surrounding fluid. Since the experimental data were necessarily provided in the form of a discrete dataset with sampling points every fifteenth of a second, a fast Fourier transform was performed on the data within MATLAB. For this initial calculation, 100 terms in the Fourier transformed signals were retained. Subsequent detailed analysis will be conducted to determine the minimum number of terms necessary to accurately model the cylinder dynamics.

The experimental data were phase averaged over many experimental trials to remove as much of the noise as possible. The resulting dataset was then used as input to the MATLAB program. Out of 225 vector fields, 50 sets were included in the ensemble. The cylinder position versus time signal was used to line up individual datasets. Phase averaging was done by centring on the peak of a beat cycle. Extensive details are provided in Dong (2002).

A comparison between the actual cylinder motion and the motion predicted by our reduced-order model is shown in figure 7. The ordinate and abscissa in the figure are shown in dimensional form. Clearly, the agreement between model and experiment is quite good. Observe that both oscillation frequency and amplitude appear to be accurately predicted by the model along with the beating behaviour. Numerical instabilities resulting from singularities when the cylinder was at points of maximum deflection are responsible for the clipping of the model result.

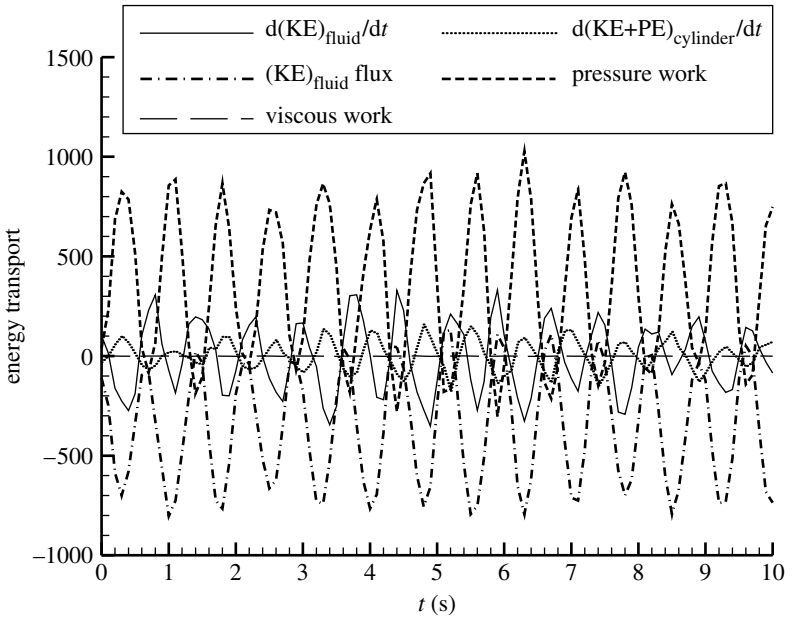

Figure 6. Phased-averaged energy terms in the integral energy transport equation for the given control volume.

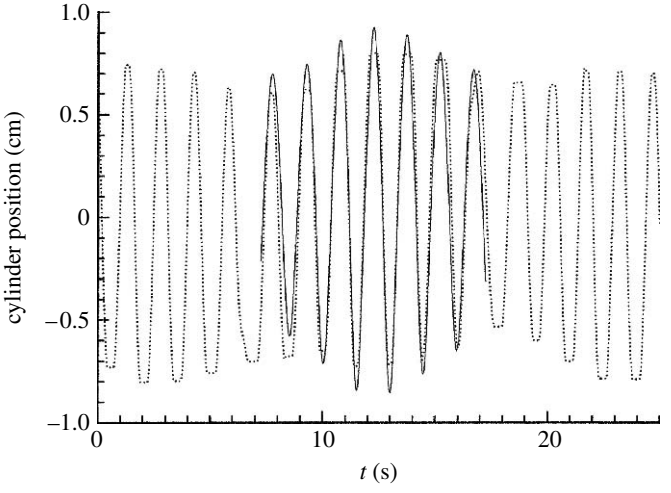

Figure 7. Comparison of the reduced-order model response (dotted line) and the phase-averaged cylinder position versus time measurements (solid line).

Experiments indicate a slight frequency mismatch between fluid kinetic energy flux and pressure work terms on one hand, and the time rate of change of the fluid kinetic energy term on the other. One can see from the individual spectra that the flux and work terms oscillate at a slightly lower frequency than the time-derivative term. One can use physical arguments coupled with detailed study of the signals to conclude that fluid kinetic energy flux and pressure work correlate with the vortex shedding while changes in fluid kinetic energy around the

cylinder follow the cylinder oscillation. Thus, we conclude that the beating phenomena observed in the resonant synchronization regime result from the competition between vortex shedding and structural vibration.

6. Advanced coupled models

We again focus on the flow of a viscous incompressible fluid around a rigid circular cylinder. A viscous incompressible fluid can be thought of as a real fluid with an internal constraint manifesting the requirement of incompressibility. In general, real fluids are holonomic and non-conservative (Leech 1977). The no-slip condition at a boundary (fluid/solid or fluid/fluid), for example, is a holonomic constraint. By holonomic it is meant that a constraint on the configuration (position) of the particles in a system of the form $G(\boldsymbol{x}, t) = 0$ exists. Time may (rheonomic) or may not (scleronomic) enter into this constraint equation explicitly.

(a) *The extended Hamilton's principle*

Consider the system of particles inhabiting the open control volume $R_\mathrm{o}(\boldsymbol{x}, t)$ at time t. This system of particles is referred to as the *open system*. Only instantaneously does it coincide with the *closed system* of particles which constitute the material system M. The control volume has a part $B_\mathrm{o}(\boldsymbol{x}, t)$ of its bounding surface $B(\boldsymbol{x}, t)$ which is open to the flow particles. The closed part of the bounding surface is $B_\mathrm{c}(\boldsymbol{x}, t)$, and includes any solid boundaries and portions of the surface in which the local streamline is normal to the surface. The kinetic energy of the open system is denoted $(\mathcal{K})_\mathrm{o}$. The sum of the gravitational potential energy $(\mathcal{E}^{(\mathrm{g})})_\mathrm{o}$, the potential energy due to buoyancy $(\mathcal{E}^{(\mathrm{b})})_\mathrm{o}$, the strain energy $(\mathcal{E}^{(\mathrm{s})})_\mathrm{o}$, and the internal energy $(\mathcal{E}^{(\mathrm{i})})_\mathrm{o}$ of the open system is denoted $(\mathcal{E})_\mathrm{o}$. $\boldsymbol{u}_\mathrm{rel}(\boldsymbol{x}, t) = \boldsymbol{u}(\boldsymbol{x}, t) - \boldsymbol{u}_\mathrm{B}$ is the fluid velocity relative to the velocity of control surface.

The extended form of Hamilton's principle for a system of changing mass (e.g. the exhaust jet of a rocket) or a system of constant mass which does not always consist of the same set of particles (e.g. a pipe of constant diameter conveying fluid) can be written as (Benaroya & Wei 2000)

$$\delta \int_{t_1}^{t_2} (\mathcal{L})_\mathrm{o}\, \mathrm{d}t + \int_{t_1}^{t_2} (\delta W)_\mathrm{o}\, \mathrm{d}t + \int_{t_1}^{t_2} \int_{B_\mathrm{o}} \int_{(t)} \rho(\boldsymbol{u}_\mathrm{rel} \cdot \delta \boldsymbol{r})(\boldsymbol{u} \cdot \boldsymbol{n}) \mathrm{d}s\, \mathrm{d}t = 0, \tag{6.1}$$

where $(\mathcal{L})_\mathrm{o} = (\mathcal{K} - \mathcal{E})_\mathrm{o}$ is the Lagrangian of the open system and $(\delta W)_\mathrm{o}$ is the virtual work performed by non-potential forces on the same system. Note that $\mathrm{d}s = \mathrm{d}s(\boldsymbol{x}, t)$ is used here to represent a differential surface element. At position $\boldsymbol{x}$ and time t, the density is ρ and the velocity is $\boldsymbol{u}$.

Note that equation (6.1) is related to the Reynolds transport theorem, which allows one to calculate time rate of change of any extensive property of system M from Eulerian measurements made inside a spatial volume which instantaneously coincides with that occupied by the mass system at time t. Designating the volume occupied by system M by $R_\mathrm{M}(\boldsymbol{x}, t)$, the open control volume instantaneously coinciding with $R_\mathrm{M}(\boldsymbol{x}, t)$ by $R_\mathrm{o}(\boldsymbol{x}, t)$, and the bounding surface of $R_\mathrm{o}(\boldsymbol{x}, t)$ by

$B(\boldsymbol{x}, t)$, the Reynolds transport theorem is given by (Malvern 1969)

$$\frac{\mathrm{D}}{\mathrm{D}t}\int\int\int_{R_{\mathrm{M}}(\boldsymbol{x},t)}\rho\mathcal{A}\,\mathrm{d}v = -\int\int_{B(\boldsymbol{x},t)}\rho\mathcal{A}(\boldsymbol{u}_{\mathrm{rel}}\cdot\mathrm{d}\boldsymbol{A})\mathrm{d}s + \int\int\int_{R_{\mathrm{o}}(\boldsymbol{x},t)}\frac{\partial}{\partial t}(\rho\mathcal{A})\mathrm{d}v. \quad (6.2)$$

In equation (6.2), $\mathcal{A}$ is an arbitrary intensive property of the system reckoned per unit mass, $\rho = \rho(\boldsymbol{x}, t)$ is the spatial density field, and $\mathrm{d}\boldsymbol{A} = \boldsymbol{n}\,\mathrm{d}s$ with $\boldsymbol{n}$ a positive *outward* normal. In the surface integral, $\boldsymbol{u}_{\mathrm{rel}}(\boldsymbol{x}, t) = \boldsymbol{u}(\boldsymbol{x}, t) - \boldsymbol{u}_B$ is the fluid velocity relative to the velocity of control surface, assumed constant in time and spatially independent if non-zero. $\boldsymbol{u}_{\mathrm{rel}}(\boldsymbol{x}, t) = \boldsymbol{0}$ on any solid boundaries, so $B(\boldsymbol{x}, t)$ in equation (6.2) is understood to exclude any such boundaries. Also excluded are any portions of the surface in which the instantaneous local streamline is normal to the surface, since in that case $\boldsymbol{u}_{\mathrm{rel}}\cdot\mathrm{d}\boldsymbol{A} = 0$.

In equation (6.1), the virtual displacements δr_i must preserve the mass balance law. This is in addition to the requirements imposed by any geometric constraints, the balance laws of internal energy and entropy, and any constitutive relations.

Suppose the *open system* is inhabited instantaneously by fluid particles moving along with the flow and a single solid body in the path of the fluid. The boundary of this solid body constitutes part of the closed boundary $B_{\mathrm{c}}(\boldsymbol{x}, t)$. The following assumptions are made.

(i) The open part of the control surface is stationary, i.e. $\boldsymbol{u}_{B_{\mathrm{o}}} = \boldsymbol{0}$. As a result, $\boldsymbol{u}_{\mathrm{rel}} = \boldsymbol{u}$.
(ii) The flow is considered to be two-dimensional. That is, all flow quantities are independent of z and $u_3(\boldsymbol{x}, t) = 0$. The vorticity is then perpendicular to the plane of motion.
(iii) The length and time scales are such that the fluid is in local thermodynamic equilibrium, even when the fluid is in motion. All macroscopic length and time scales are considerably larger than the largest molecular length and time scales.
(iv) An inertial rectangular Cartesian coordinate system is used, with basis vectors $\boldsymbol{e}_1$, $\boldsymbol{e}_2$ and $\boldsymbol{e}_3$ in the x, y and z-directions, respectively.
(v) The resultant of all body forces, both conservative and non-conservative, in the open control volume is assumed small. As a consequence of this assumption, the gravitational and buoyancy effects are neglected and $(\mathcal{E}^{(\mathrm{g})})_{\mathrm{o}} = (\mathcal{E}^{(\mathrm{b})})_{\mathrm{o}} = 0$.
(vi) Changes in the internal energy $\mathrm{D}(\mathcal{E}^{(\mathrm{i})})_{\mathrm{o}}/\mathrm{D}t$, which are entirely due to the motion of the fluid, are neglected. As a consequence of the commutative property of the operators $\delta(\cdot)$ and $\mathrm{D}(\cdot)/\mathrm{D}t$, this is equivalent to

$$\delta(\mathcal{E}^{(\mathrm{i})})_{\mathrm{o}} = \delta\left(\mathcal{E}^{(\mathrm{i})}_{\mathrm{fluid}}\right)_{\mathrm{o}} = \delta\int\int\int_{R_{\mathrm{o}}(\boldsymbol{x},t)}\rho e(\rho, T)\mathrm{d}v = 0, \quad (6.3)$$

where e is the specific internal energy and $T(\boldsymbol{x}, t)$ is the thermodynamic temperature field. Note that $e(\rho, T)$ is the so-called caloric equation of state (Malvern 1969).

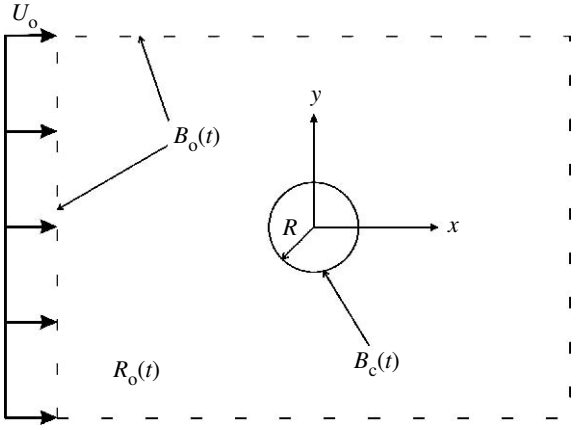

Figure 8. The open control surface $B_o(t)$, the closed control surface $B_c(t)$ and the open control volume $R_o(t)$. Reference is made to the case of uniform flow U_o past a stationary circular cylinder of radius R.

While the fluid is initially allowed to be compressible, potentially rendering this last assumption invalid, subsequent application of the incompressibility approximation vindicates said assumption.

Finally, the dependence of R_o, B_o, and B_c on $\boldsymbol{x}$ is omitted from here on since it is understood that these variables refer to the spatial description. The dependencies of ρ and $\boldsymbol{u}$ on $\boldsymbol{x}$ and t are also dropped.

(*b*) *Uniform viscous flow past a stationary cylinder*

Let the control volume be defined as the rectangular volume of unit depth surrounding the stationary cylinder. The origin of the coordinate system is at the centre of the cylinder. The part of the control surface that is pervious represents a significant portion of the outer surface defined by the perimeter of the rectangle shown in figure 8 multiplied by a unit projection out of the plane of said figure. This part is the *open control surface* $B_o(t)$. The *closed control surface* $B_c(t)$, includes the circumference of the cylinder $x^2 + y^2 = R^2$, and any portions of the outer surface that are closed to fluid motion (i.e. those portions where $\boldsymbol{u}(\boldsymbol{x}, t) \| \boldsymbol{n}$).

Note that in this particular problem, the surfaces $B_o(t)$ and $B_c(t)$ are functions of neither time nor space. This obviously means that the open control volume $R_o(t)$ is also independent of time and space. The CV and CS definitions are illustrated in figure 8. The open control volume, $R_o(t)$, is clearly of constant mass, yet it does not consist of the same set of particles at any two instances. The uniform, steady free-stream velocity is $\boldsymbol{u}_o = U_o \boldsymbol{e}_1$.

The kinetic energy of the open system is given by

$$(\mathcal{K})_o = (\mathcal{K}_{\text{fluid}})_o = \int\int\int_{R_o(t)} \frac{1}{2}\rho(\boldsymbol{u}\cdot\boldsymbol{u})\mathrm{d}v, \tag{6.4}$$

where $\mathrm{d}v = \mathrm{d}v(\boldsymbol{x}, t)$ is the differential volume element. For the sake of brevity, the functional dependencies of $\mathrm{d}v$ and $\mathrm{d}s$ are dropped. Clearly $(\mathcal{K}_{\text{cyl}})_o = 0$. Also, $(\mathcal{E}^{(s)})_o = 0$ since the cylinder is rigid. From equation (6.3), and the additional

relations $(\mathcal{E}^{(\mathrm{g})})_{\mathrm{o}} = (\mathcal{E}^{(\mathrm{b})})_{\mathrm{o}} = 0$, $\delta(\mathcal{E})_{\mathrm{o}} = 0$, it follows that

$$\delta \int_{t_1}^{t_2} (\mathcal{L})_{\mathrm{o}}\, \mathrm{d}t = \delta \int_{t_1}^{t_2} (\mathcal{K})_{\mathrm{o}}\, \mathrm{d}t = \delta \int_{t_1}^{t_2} \iiint_{R_{\mathrm{o}}(t)} \frac{1}{2}\rho(\boldsymbol{u}\cdot\boldsymbol{u})\mathrm{d}v\, \mathrm{d}t. \tag{6.5}$$

The virtual work done by the normal and tangential stresses in the fluid during a virtual displacement is given by (Dost & Tabarrok 1979)

$$(\delta W)_{\mathrm{o}} = (\delta W_{\mathrm{fluid}})_{\mathrm{o}} = -\iiint_{R_{\mathrm{o}}(t)} \sigma_{ij}\delta\varepsilon_{ij}\, \mathrm{d}v, \tag{6.6}$$

where σ_{ij} is the natural or Eulerian stress tensor and

$$\delta\varepsilon_{ij} = \frac{1}{2}\left[\frac{\partial(\delta r_j)}{\partial x_i} + \frac{\partial(\delta r_i)}{\partial x_j}\right]. \tag{6.7}$$

It is tempting to regard $\delta\varepsilon_{ij}$ as the Lagrangian variation of Cauchy's infinitesimal (linear) strain tensor,

$$\varepsilon_{ij} = \frac{1}{2}\left[\frac{\partial r_i}{\partial x_j} + \frac{\partial r_j}{\partial x_i}\right].$$

However,

$$\delta\varepsilon_{ij} = \frac{1}{2}\left[\delta\left(\frac{\partial r_i}{\partial x_j}\right) + \delta\left(\frac{\partial r_j}{\partial x_i}\right)\right] \neq \frac{1}{2}\left[\frac{\partial(\delta r_i)}{\partial x_j} + \frac{\partial(\delta r_j)}{\partial x_i}\right].$$

The balance of angular momentum applied to a differential fluid volume element $\mathrm{d}v = \mathrm{d}x\, \mathrm{d}y(\mathrm{d}z = 1)$ leads to the conclusion that the stress tensor is symmetric, $\sigma_{ij} = \sigma_{ji}$. Using this symmetry property it can be easily shown that

$$\frac{1}{2}\sigma_{ij}\left[\frac{\partial(\delta r_j)}{\partial x_i} + \frac{\partial(\delta r_i)}{\partial x_j}\right] = \sigma_{ij}\left[\frac{\partial(\delta r_i)}{\partial x_j}\right].$$

As a consequence, equation (6.6) becomes

$$(\delta W)_{\mathrm{o}} = -\iiint_{R_{\mathrm{o}}(t)} \sigma_{ij}\left[\frac{\partial(\delta r_i)}{\partial x_j}\right]\mathrm{d}v. \tag{6.8}$$

Using equations (6.5) and (6.8), equation (6.1) can be written as

$$\delta \int_{t_1}^{t_2} \iiint_{R_{\mathrm{o}}(t)} \frac{1}{2}\rho(\boldsymbol{u}\cdot\boldsymbol{u})\mathrm{d}v\, \mathrm{d}t - \int_{t_1}^{t_2} \iiint_{R_{\mathrm{o}}(t)} \sigma_{ij}\left[\frac{\partial(\delta r_i)}{\partial x_j}\right]\mathrm{d}v\, \mathrm{d}t$$
$$+ \int_{t_1}^{t_2} \iint_{B_{\mathrm{o}}(t)} \rho(\boldsymbol{u}\cdot\delta\boldsymbol{r})(\boldsymbol{u}\cdot\boldsymbol{n})\mathrm{d}s\, \mathrm{d}t = 0. \tag{6.9}$$

Before proceeding with the development of equation (6.9), the components σ_{ij} of the stress tensor $\boldsymbol{\sigma}$ that appear in equation (6.9) are defined.

(c) The stress tensor

It can be shown that the constitutive relation relating the stress tensor σ to the density field $\rho(\boldsymbol{x}, t)$, the thermodynamic pressure field $p(\boldsymbol{x}, t)$, and the velocity gradient tensor $\mathsf{L} = [\nabla \boldsymbol{u}(\boldsymbol{x}, t)]^{\mathrm{T}}$ in a Newtonian fluid is given by (Currie 2003)

$$\sigma = [-p + \lambda(\nabla \cdot \boldsymbol{u})]\mathsf{I} + \mu\left[(\nabla \boldsymbol{u}) + (\nabla \boldsymbol{u})^{\mathrm{T}}\right], \tag{6.10}$$

where I is the identity tensor. The operator ∇ is understood to be a spatial operator, i.e. $\nabla \equiv \nabla_{\boldsymbol{x}}$. The thermodynamic pressure field is defined by the equation of state

$$p = p(\rho, T).$$

The Cartesian components of equation (6.10) are

$$\sigma_{ij} = -p\delta_{ij} + \lambda\delta_{ij}\frac{\partial u_k}{\partial x_k} + \mu\left(\frac{\partial u_i}{\partial x_j} + \frac{\partial u_j}{\partial x_i}\right). \tag{6.11}$$

The parameters μ and λ are usually referred to as the dynamic viscosity coefficient and the second viscosity coefficient, respectively. From assumption (iii) of §6*a*, it is possible to make an important simplification: $\mu = \mu(\rho, T)$ and $\lambda = \lambda(\rho, T)$ depend only on the equilibrium properties of ρ and T. Here, the additional simplification is made that μ and λ are effectively constant.

Equation (6.10) follows from the general form:

$$\sigma = -p\mathsf{I} + \boldsymbol{G}(\nabla \boldsymbol{u}), \tag{6.12}$$

where $\boldsymbol{G}$ is a *linear* tensor valued function. $\nabla \boldsymbol{u}$ can be written as the sum of a symmetric tensor D and a skew-symmetric tensor W, which are defined by

$$\mathsf{D} = \frac{1}{2}\left[(\nabla \boldsymbol{u}) + (\nabla \boldsymbol{u})^{\mathrm{T}}\right]$$

$$\mathsf{W} = \frac{1}{2}\left[(\nabla \boldsymbol{u}) - (\nabla \boldsymbol{u})^{\mathrm{T}}\right].$$

The tensors D and W are the rate of deformation and spin tensor, respectively.

Using these tensors, equation (6.12) can then be written as

$$\sigma = -p\mathsf{I} + \boldsymbol{G}(\mathsf{D} + \mathsf{W}).$$

In a rigid body rotation of the fluid there can be no shear stresses since there is no shearing action. The shear stresses are represented entirely by the components of tensor W. Since these components are non-zero for a rigid body rotation, it is clear that σ must be independent of W. Assuming the fluid is isotropic, then $\boldsymbol{G}(\mathsf{D})$ can be written as (Malvern 1969)

$$\boldsymbol{G}(\mathsf{D}) = \lambda(\mathrm{tr}\,\mathsf{D})\mathsf{I} + 2\mu\mathsf{D},$$

where tr D is the trace of D.

The stress tensor can now be expressed as

$$\sigma = -p\mathsf{I} + \lambda(\mathrm{tr}\,\mathsf{D})\mathsf{I} + 2\mu\mathsf{D}. \tag{6.13}$$

The variation of the first term of equation (6.9), representing the variation of the total fluid kinetic energy in the open control volume, is intimately related to variational form of the integral or global mass balance law.

(*d*) *The global mass balance law*

Regarding the mass balance law, McIver (1973) states that the necessary condition in integral form becomes

$$\delta \int\int\int_{R_o(t)} \rho(\cdot)\mathrm{d}v = \int\int\int_{R_o(t)} \rho\delta(\cdot)\mathrm{d}v, \tag{6.14}$$

where $(\cdot)$ is an arbitrary function of $\boldsymbol{x}$ and t. The origin of equation (6.14) lies in the statement of global mass balance for mass system M, which occupies the volume $R_M(t)$ at time t. In variational form, this is given by (Xing & Price 1997)

$$\delta \int\int\int_{R_M(t)} \rho(\cdot)\mathrm{d}v = \int\int\int_{R_M(t)} \rho\delta(\cdot)\mathrm{d}v. \tag{6.15}$$

Recall that system M is closed. That is, it always consists of the same collection of particles and there is no mass transport through its surface. Its bounding surface $B_M(t)$ moves with translational velocity $N = u_i n_i$ which is the same as the local fluid velocity.

McIver (1973) argues that as far as the operator δ is concerned, equations (6.14) and (6.15) are equivalent at the instant when $R_M(t)$ and $R_o(t)$ coincide. He describes this correspondence as:

> The control volume, open or closed, is always a closed system as far as the variation is concerned regardless of whether or not material is transported across its boundaries in the real motion: there is no virtual material transport out of the system.

The continuity equation

$$\frac{\mathrm{D}\rho}{\mathrm{D}t} + \rho\left(\frac{\partial u_k}{\partial x_k}\right) = \frac{\partial \rho}{\partial t} + \frac{\partial(\rho u_k)}{\partial x_k} = 0, \tag{6.16}$$

representing the local mass conservation law, is in fact a necessary condition for equation (6.15).

(*e*) *The kinetic energy*

The first term in equation (6.10) can be written as

$$\begin{aligned}\delta \int_{t_1}^{t_2} \int\int\int_{R_o(t)} \rho(\boldsymbol{u}\cdot\boldsymbol{u})\mathrm{d}v\,\mathrm{d}t &= \int_{t_1}^{t_2} \int\int\int_{R_o(t)} \rho(\boldsymbol{u}\cdot\delta\boldsymbol{u})\mathrm{d}v\,\mathrm{d}t \\ &= \int_{t_1}^{t_2} \int\int\int_{R_o(t)} \rho\left[\boldsymbol{u}\cdot\delta\left(\frac{\mathrm{D}\boldsymbol{r}}{\mathrm{D}t}\right)\right]\mathrm{d}v\,\mathrm{d}t.\end{aligned} \tag{6.17}$$

Using the fact that the variation denoted by the operator $\delta(\cdot)$ and the rate of change denoted by $\mathrm{D}(\cdot)/\mathrm{D}t$ are both material variations and are consequently

interchangeable, equation (6.17) can be written as

$$\int_{t_1}^{t_2}\iiint_{R_o(t)}\rho\left[\boldsymbol{u}\cdot\delta\left(\frac{\mathrm{D}\boldsymbol{r}}{\mathrm{D}t}\right)\right]\mathrm{d}v\,\mathrm{d}t=\int_{t_1}^{t_2}\iiint_{R_o(t)}\rho\left[\boldsymbol{u}\cdot\frac{\mathrm{D}(\delta\boldsymbol{r})}{\mathrm{D}t}\right]\mathrm{d}v\,\mathrm{d}t. \tag{6.18}$$

Consider next the following result from Dost & Tabarrok (1979):

$$\begin{aligned}\int_{t_1}^{t_2}\frac{\mathrm{D}}{\mathrm{D}t}\left[\iiint_{R_o(t)}\rho(\boldsymbol{u}\cdot\delta\boldsymbol{r})\mathrm{d}v\right]\mathrm{d}t&=\int_{t_1}^{t_2}\iiint_{R_o(t)}\rho\left[\boldsymbol{u}\cdot\frac{\mathrm{D}(\delta\boldsymbol{r})}{\mathrm{D}t}\right]\mathrm{d}v\,\mathrm{d}t\\&\quad+\int_{t_1}^{t_2}\iiint_{R_o(t)}\left(\frac{\mathrm{D}\rho}{\mathrm{D}t}+\rho\nabla\cdot\boldsymbol{u}\right)\mathrm{d}v\,\mathrm{d}t\\&\quad+\int_{t_1}^{t_2}\iiint_{R_o(t)}\rho\left(\frac{\mathrm{D}\boldsymbol{u}}{\mathrm{D}t}\cdot\delta\mathrm{r}\right)\mathrm{d}v\,\mathrm{d}t.\end{aligned}$$

On account of the continuity equation, equation (6.16), the second integral vanishes, and

$$\begin{aligned}\int_{t_1}^{t_2}\frac{\mathrm{D}}{\mathrm{D}t}\left[\iiint_{R_o(t)}\rho(\boldsymbol{u}\cdot\delta\boldsymbol{r})\mathrm{d}v\right]\mathrm{d}t&=\int_{t_1}^{t_2}\iiint_{R_o(t)}\rho\left[\boldsymbol{u}\cdot\frac{\mathrm{D}(\delta\boldsymbol{r})}{\mathrm{D}t}\right]\mathrm{d}v\,\mathrm{d}t\\&\quad+\int_{t_1}^{t_2}\iiint_{R_o(t)}\rho\left(\frac{\mathrm{D}\boldsymbol{u}}{\mathrm{D}t}\cdot\delta\boldsymbol{r}\right)\mathrm{d}v\,\mathrm{d}t.\end{aligned}$$

Replacing

$$\begin{aligned}\int_{t_1}^{t_2}\iiint_{R_o(t)}\rho\left[\boldsymbol{u}\cdot\frac{\mathrm{D}(\delta\boldsymbol{r})}{\mathrm{D}t}\right]\mathrm{d}v\,\mathrm{d}t&=\int_{t_1}^{t_2}\frac{\mathrm{D}}{\mathrm{D}t}\left[\iiint_{R_o(t)}\rho(\boldsymbol{u}\cdot\delta\boldsymbol{r})\mathrm{d}v\right]\mathrm{d}t\\&\quad-\int_{t_1}^{t_2}\iiint_{R_o(t)}\rho\left(\frac{\mathrm{D}\boldsymbol{u}}{\mathrm{D}t}\cdot\delta\boldsymbol{r}\right)\mathrm{d}v\,\mathrm{d}t\end{aligned}$$

in equation (6.17) leads to

$$\begin{aligned}\int_{t_1}^{t_2}\iiint_{R_o(t)}\rho\left[\boldsymbol{u}\cdot\delta\left(\frac{\mathrm{D}\boldsymbol{r}}{\mathrm{D}t}\right)\right]\mathrm{d}v\,\mathrm{d}t&=\int_{t_1}^{t_2}\frac{\mathrm{D}}{\mathrm{D}t}\left[\iiint_{R_o(t)}\rho(\boldsymbol{u}\cdot\delta\boldsymbol{r})\mathrm{d}v\right]\mathrm{d}t\\&\quad-\int_{t_1}^{t_2}\iiint_{R_o(t)}\rho\left(\frac{\mathrm{D}\boldsymbol{u}}{\mathrm{D}t}\cdot\delta\boldsymbol{r}\right)\mathrm{d}v\,\mathrm{d}t.\end{aligned} \tag{6.19}$$

Integrating the first term of equation (6.19) gives

$$\left[\iiint_{R_o(t)}\rho(\boldsymbol{u}\cdot\delta\boldsymbol{r})\mathrm{d}v\right]_{t_1}^{t_2},$$

which vanishes on account of the constraint $\delta\boldsymbol{r}(t_1)=\delta\boldsymbol{r}(t_2)=0$. Equation (6.19) is then simply

$$\begin{aligned}\delta\int_{t_1}^{t_2}\iiint_{R_o(t)}\rho(\boldsymbol{u}\cdot\boldsymbol{u})\mathrm{d}v\,\mathrm{d}t&=\int_{t_1}^{t_2}\iiint_{R_o(t)}\rho\left[\boldsymbol{u}\cdot\delta\left(\frac{\mathrm{D}\boldsymbol{r}}{\mathrm{D}t}\right)\right]\mathrm{d}v\,\mathrm{d}t\\&=-\int_{t_1}^{t_2}\iiint_{R_o(t)}\rho\left(\frac{\mathrm{D}\boldsymbol{u}}{\mathrm{D}t}\cdot\delta\boldsymbol{r}\right)\mathrm{d}v\,\mathrm{d}t.\end{aligned} \tag{6.20}$$

Replacing equation (6.20) in equation (6.9) yields

$$-\int_{t_1}^{t_2}\iiint_{R_o(t)}\rho\left(\frac{\mathrm{D}\boldsymbol{u}}{\mathrm{D}t}\cdot\delta\boldsymbol{r}\right)\mathrm{d}v\,\mathrm{d}t-\int_{t_1}^{t_2}\iiint_{R_o(t)}\sigma_{ij}\left[\frac{\partial(\delta r_i)}{\partial x_j}\right]\mathrm{d}v\,\mathrm{d}t$$
$$+\int_{t_1}^{t_2}\iint_{B_o(t)}\rho(\boldsymbol{u}\cdot\delta\boldsymbol{r})(\boldsymbol{u}\cdot\boldsymbol{n})\mathrm{d}s\,\mathrm{d}t=0. \tag{6.21}$$

(*f*) *Virtual work*

Having obtained the variation of the kinetic energy of the fluid, which in the present case represents the Lagrangian of the open system, attention is now focused on the virtual work. The second term of equation (6.21) can be expressed in the equivalent form

$$\int_{t_1}^{t_2}\iiint_{R_o(t)}\sigma_{ij}\left[\frac{\partial(\delta r_i)}{\partial x_j}\right]\mathrm{d}v\,\mathrm{d}t=\int_{t_1}^{t_2}\iiint_{R_o(t)}\left[\frac{\partial(\sigma_{ij}\delta r_i)}{\partial x_j}-\frac{\partial\sigma_{ij}}{\partial x_j}\delta r_i\right]\mathrm{d}v\,\mathrm{d}t. \tag{6.22}$$

The divergence theorem is used to transform the first term inside the integral.

The divergence theorem for a (sufficiently well-behaved) vector field $\boldsymbol{w}$ is given in Cartesian form by

$$\iint_{B(t)}w_in_i\,\mathrm{d}s=\iiint_{R_o(t)}\frac{\partial w_i}{\partial x_i}\mathrm{d}v, \tag{6.23}$$

where $B(t)$ is the bounding surface of region $R_o(t)$.

Applying equation (6.23) with $\boldsymbol{w}=\boldsymbol{\sigma}^{\mathrm{T}}\delta\boldsymbol{r}$, i.e. $w_i=\sigma_{ij}\delta r_i$, the following form of equation (6.22) is obtained:

$$\int_{t_1}^{t_2}\iiint_{R_o(t)}\left[\frac{\partial(\sigma_{ij}\delta r_i)}{\partial x_j}-\frac{\partial\sigma_{ij}}{\partial x_j}\delta r_i\right]\mathrm{d}v\,\mathrm{d}t$$
$$=\int_{t_1}^{t_2}\iint_{B(t)}\sigma_{ij}n_j\delta r_i\,\mathrm{d}s\,\mathrm{d}t-\int_{t_1}^{t_2}\iiint_{R_o(t)}\left[\frac{\partial\sigma_{ij}}{\partial x_j}\delta r_i\right]\mathrm{d}v\,\mathrm{d}t. \tag{6.24}$$

Using equation (6.24), equation (6.21) becomes

$$-\int_{t_1}^{t_2}\iiint_{R_o(t)}\rho\left(\frac{\mathrm{D}\boldsymbol{u}}{\mathrm{D}t}\cdot\delta\boldsymbol{r}\right)\mathrm{d}v\,\mathrm{d}t+\int_{t_1}^{t_2}\iiint_{R_o(t)}\left[\frac{\partial\sigma_{ij}}{\partial x_j}\delta r_i\right]\mathrm{d}v\,\mathrm{d}t$$
$$-\int_{t_1}^{t_2}\iint_{B(t)}\sigma_{ij}n_j\delta r_i\,\mathrm{d}s\,\mathrm{d}t+\int_{t_1}^{t_2}\iint_{B_o(t)}\rho(\boldsymbol{u}\cdot\delta\boldsymbol{r})(\boldsymbol{u}\cdot\boldsymbol{n})\mathrm{d}s\,\mathrm{d}t=0, \tag{6.25}$$

where $B(t)=B_o(t)\cup B_c(t)$ and $\boldsymbol{n}$ is the outward normal. Note that $\boldsymbol{n}$ points *into* the cylinder on surface $B_c(t)$. It must be emphasized that in using the divergence theorem to convert equation (6.22) to equation (6.24), a subtlety arises. The domain $R_o(t)$ is actually doubly connected.

(i) *The doubly connected domain*

In fact, the region occupied by the fluid in a two-dimensional flow field due to *any* moving body is necessarily doubly connected (Batchelor 1967). A problem arises in the direct application of the divergence theorem. However, this problem is easily dealt with by defining the bounding surface of $R_o(t)$ to be $B^*(t) = B_o(t) \cup B_c(t) \cup B_u(t)$, where $B_u(t)$ is the surface of the umbilicus (branch cut) which joins the exterior surface $B_o(t)$ to the body surface $B_c(t)$. This is illustrated in figure 9. It can be shown that integration of $\boldsymbol{\sigma n}$ over the umbilicus does not contribute to the total surface integral (Noca 1997). Thus, $B^*(t)$ may be effectively taken as equal to $B(t)$.

(g) *The Euler–Lagrange equations and the natural boundary conditions*

Collecting like terms in equation (6.25) gives

$$\int_{t_1}^{t_2} \iiint_{R_o(t)} \left[-\rho \frac{\mathrm{D}u_i}{\mathrm{D}t} + \frac{\partial \sigma_{ij}}{\partial x_j} \right] \delta r_i \, \mathrm{d}v \, \mathrm{d}t - \int_{t_1}^{t_2} \iint_{B_c(t)} \sigma_{ij} n_j \delta r_i \, \mathrm{d}s \, \mathrm{d}t$$

$$- \int_{t_1}^{t_2} \iint_{B_o(t)} \left[\sigma_{ij} n_j - \rho u_i u_j n_j \right] \delta r_i \, \mathrm{d}v \, \mathrm{d}t = 0.$$

Arguing in the usual way that the variations δr_i are arbitrary in $R_o(t) \times [t_1, t_2]$ leads to the Euler–Lagrange (EL) equation

$$\rho \frac{\mathrm{D}u_i}{\mathrm{D}t} = \frac{\partial(\sigma_{ij})}{\partial x_j} \quad \text{in} \quad R_o(t). \tag{6.26}$$

A similar argument regarding the variations δr_i on $B_o(t) \times [t_1, t_2]$ and $B_c(t) \times [t_1, t_2]$ leads to the natural boundary conditions

$$\sigma_{ij} n_j \delta r_i = 0 \quad \text{on} \quad B_c(t) \tag{6.27}$$

and

$$[\sigma_{ij} n_j - \rho u_i u_j n_j] \delta r_i = 0 \quad \text{on} \quad B_o(t). \tag{6.28}$$

Substituting equation (6.11) into equation (6.26) yields the components of the balance of linear momentum equation for a Newtonian viscous compressible fluid with constant viscosity coefficients

$$\rho \frac{\mathrm{D}u_i}{\mathrm{D}t} = -\frac{\partial p}{\partial x_i} + \lambda \left(\frac{\partial^2 u_j}{\partial x_i \, \partial x_j} \right) + \mu \left[\frac{\partial}{\partial x_j} \left(\frac{\partial u_i}{\partial x_j} + \frac{\partial u_j}{\partial x_i} \right) \right] \quad \text{in} \quad R_o(t). \tag{6.29}$$

The next step is to use Stokes' condition, $\lambda = -2\mu/3$. Stokes' condition is equivalent to the assumption that the thermodynamic pressure and the mechanical pressure are the same for a compressible fluid.

To see this, consider the difference between the thermodynamic pressure p and the mean mechanical pressure $\bar{p}_m$ (Malvern 1969),

$$p - \bar{p}_m = -\left(\lambda + \frac{2}{3}\mu \right) \frac{\partial u_k}{\partial x_k} = -\left(\lambda + \frac{2}{3}\mu \right) \frac{1}{\rho} \frac{\mathrm{D}\rho}{\mathrm{D}t}, \tag{6.30}$$

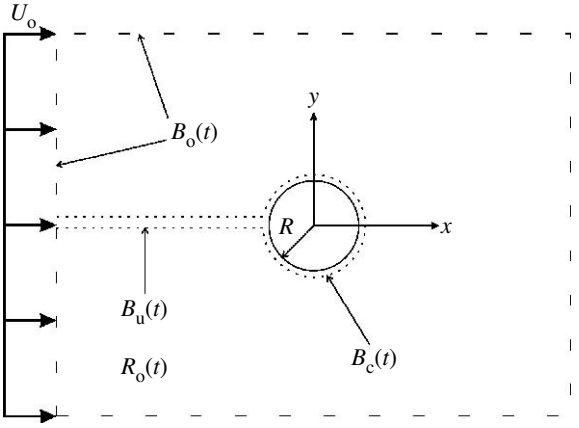

Figure 9. The open control surface $B_o(t)$, closed control surface $B_c(t)$, the umbilicus $B_u(t)$ and the open control volume $R_o(t)$. Reference is made to the case of uniform flow U_o past a stationary circular cylinder of radius R.

where the last equality follows from the continuity equation, equation (6.16). In equation (6.29), the mean mechanical pressure is defined as

$$\bar{p}_m = -\frac{1}{3}\sigma_{ii}.$$

In a fluid at rest the stress is purely hydrostatic, $\sigma_{ij} = -\bar{p}_m \delta_{ij}$, and consequently $\bar{p}_m = p$.

Since $D\rho/Dt \neq 0$ for a compressible fluid, the thermodynamic and mechanical pressures can only be the same if the coefficient is equal to zero, $(\lambda + (2/3)\mu) = 0$. The quantity $(\lambda + (2/3)\mu) = \mu_B$ is usually referred to as the bulk viscosity. The vanishing of the bulk viscosity has an interesting interpretation: the dissipation power per unit volume is due entirely to shape change rate of deformation. The volume change or dilatational dissipation is zero (Malvern 1969). It can be shown that in order to satisfy the Clausius–Duhem entropy inequality, $\mu \geq 0$ and $(\lambda + 2\mu/3) \geq 0$.

Using Stokes' condition, equation (6.29) becomes

$$\rho \frac{Du_i}{Dt} = -\frac{\partial p_m}{\partial x_i} - \frac{2\mu}{3}\left(\frac{\partial^2 u_j}{\partial x_i\, \partial x_j}\right) + \mu\left[\frac{\partial}{\partial x_j}\left(\frac{\partial u_i}{\partial x_j} + \frac{\partial u_j}{\partial x_i}\right)\right] \quad \text{in} \quad R_o(t). \tag{6.31}$$

Expanding the last term of equation (6.31) and combining with the second gives

$$\rho \frac{Du_i}{Dt} = -\frac{\partial p_m}{\partial x_i} + \mu\left(\frac{\partial^2 u_k}{\partial x_k^2}\right) + \frac{1}{3}\mu\left[\frac{\partial}{\partial x_i}\left(\frac{\partial u_k}{\partial x_k}\right)\right] \quad \text{in} \quad R_o(t). \tag{6.32}$$

In summary, equation (6.32) gives the components of the Navier–Stokes (N–S) equation for a compressible fluid with no bulk viscosity. Similarly, equation (6.31) gives the components of the generalized N–S equation for a compressible fluid with bulk viscosity.

(*h*) *The application to an incompressible fluid*

An incompressible fluid is a fluid in which the density of each material element is unaffected by changes in pressure. This definition holds provided that density changes in the fluid as a result of molecular conduction of heat are negligible (Batchelor 1967). In an incompressible fluid, the mean mechanical pressure is equal to the thermodynamic pressure at all times. This result follows directly from equation (6.30), since the rate of change of ρ following a material element is zero, $\mathrm{D}\rho/\mathrm{D}t=0$. The simplified continuity equation,

$$\frac{\partial u_k}{\partial x_k} = 0, \tag{6.33}$$

when used to simplify equation (6.32) leads to

$$\rho\left(\frac{\partial u_i}{\partial t} + u_j \frac{\partial u_i}{\partial x_j}\right) = -\frac{\partial p}{\partial x_i} + \mu \frac{\partial^2 u_i}{\partial x_j^2} \quad \text{in} \quad R_{\mathrm{o}}(t). \tag{6.34}$$

Note that in equation (6.34) the material derivative $\mathrm{D}u_i/\mathrm{D}t$ has been expanded. Equation (6.34) represents the components of the Navier–Stokes equation for viscous incompressible flows.

For convenience, let the stress tensor for incompressible Newtonian fluid be denoted as $\hat{\boldsymbol{\sigma}}$. Using the continuity equation, equation (6.33), to simplify the constitutive relation, equation (6.11), the components of $\hat{\boldsymbol{\sigma}}$ are given by

$$\hat{\sigma}_{ij} = -p\delta_{ij} + \mu\left(\frac{\partial u_i}{\partial x_j} + \frac{\partial u_j}{\partial x_i}\right). \tag{6.35}$$

The natural boundary condition manifested in equation (6.27) is interpreted as $\delta r_i=0$ on $B_{\mathrm{c}}(t)$ since the displacement $r_i=0$ is prescribed on the cylinder surface. However, there is no local equilibrium on the cylinder surface $\hat{\sigma}_{ij}n_j \neq 0$. The natural boundary condition manifested in equation (6.28) is interpreted as $[\hat{\sigma}_{ij}n_j - \rho u_i u_j n_j] = 0$ on $B_{\mathrm{o}}(t)$, since the displacement δr_i is not prescribed anywhere on this surface. Physically, this last boundary condition states that convective flux of momentum (per unit area as $\mathrm{d}s$ shrinks to a point) $\rho u_i u_j n_j$ at any point on $B_{\mathrm{o}}(t)$ is equal to the resultant contact force $t_i = \hat{\sigma}_{ij}n_j$ exerted at that boundary point by the surrounding matter.

(*i*) *An examination of the boundary condition manifested by equation* (*6.28*)

To better understand the meaning of this last boundary condition, consider the balance of momentum in integral form for an incompressible fluid

$$\int\int\int_{R_{\mathrm{o}}(t)} \frac{\partial(\rho u_i)}{\partial t}\,\mathrm{d}v = -\int\int_{B(t)} \rho u_i u_j n_j\,\mathrm{d}s + \int\int_{B(t)} \hat{\sigma}_{ij}n_j\,\mathrm{d}s. \tag{6.36}$$

Equation (6.28) implies that

$$\int\int_{B_{\mathrm{o}}(t)} [\hat{\sigma}_{ij}n_j - \rho u_i u_j n_j]\mathrm{d}s = 0.$$

Consequently, equation (6.36) becomes

$$\int\int\int_{R_o(t)} \frac{\partial(\rho u_i)}{\partial t}\,\mathrm{d}v = -\int\int_{B_c(t)} \rho u_i u_j n_j\,\mathrm{d}s + \int\int_{B_c(t)} \hat{\sigma}_{ij} n_j\,\mathrm{d}s. \tag{6.37}$$

Now for a stationary rigid cylinder $u_1 = u_2 = 0$ and the first integral on the r.h.s. vanishes. This integral also vanishes for a rigid cylinder in motion since the velocity components u_i on the surface of the cylinder are independent of position along the circumference cylinder (along each point on this path they must equal the velocity components V_i of the body) and

$$\int\int_{B_c(t)} \boldsymbol{n}\,\mathrm{d}s = \mathbf{0}.$$

Equation (6.37) becomes

$$\int\int\int_{R_o(t)} \frac{\partial(\rho u_i)}{\partial t}\,\mathrm{d}v = \int\int_{B_c(t)} \hat{\sigma}_{ij} n_j\,\mathrm{d}s.$$

This result can be interpreted as follows: the rate of change of momentum inside the chosen control volume is due entirely to the resultant force system at the boundary of the cylinder! The validity of this result is in general only for infinite domains $R_\infty(t)$ enclosing all of the vorticity. The surface integrals of the viscous and convective terms must also vanish at infinity.

Under these conditions, it can be shown (Noca 1997) that the balance of momentum equation, equation (6.37), reduces to a form that does not include contributions from the outer boundary at infinity. This is because a boundary term arises upon the conversion of the l.h.s. of equation (6.36) to a vorticity impulse-type term which cancels out the non-zero pressure term on the distant boundary, $-\int\int_{B_\infty(t)} p n_j\,\mathrm{d}s$. Since it is assumed that $B_o(t)$ is sufficiently far away from the cylinder such that the above conditions are satisfied, the boundary condition on $B_o(t)$ obtained above is valid.

This completes the derivation of the relevant field equations and boundary conditions for the flow of a viscous incompressible fluid past a stationary cylinder. The starting point of the derivation was Hamilton's principle for a system of variable mass. In §7, the cylinder is allowed to move freely in the direction transverse to the flow. The cylinder responds to the vortex shedding, which generates unsteady forces on the cylinder. When the frequency of the vortex shedding f_{vs} matches the cylinder oscillation frequency f_{ex}, synchronization takes place and the cylinder can undergo large oscillations. A more detailed discussion on vortex-induced vibration of circular cylinders can be found in various recent review papers, including Sarpkaya (2004), Williamson & Govardhan (2004) and Gabbai & Benaroya (2005).

7. Uniform two-dimensional viscous flow past a cylinder free to move transversely

Consider an elastically mounted cylinder, with a mechanical restraint preventing motion in the flow direction (x). Since the cylinder is rigid, its motion in the transverse direction (y) can be described by a single generalized coordinate. Let

this generalized coordinate be represented by χ. Assuming perfect correlation of the shedding vortices, the transverse displacement of all points on the cylinder is the same, $\chi = \chi(t)$. The horizontal plane passing through the cylinder's centre of mass is chosen as the reference plane and all dynamic variables (i.e. displacement, velocity, acceleration) are thus defined at the centre of mass. The total stiffness of the supporting springs is $k_{\mathrm{s}}^{(\chi)}$. The mass of the cylinder is m_{c}.

The goal here is to obtain the equations of motion for both the cylinder and the fluid in the CV. It is obvious that the equations of motion must be coupled. The motion of the cylinder must have an effect on the fluid flowing around it and vice versa.

Again, let the CV be defined as the rectangular volume surrounding the non-stationary cylinder. The origin of the coordinate system is at the centre of the cylinder when the cylinder is at rest. The coordinate system does *not* move with the cylinder and is considered to be at rest relative to the free-stream. As in §6*b*, the open part of the CS, $B_{\mathrm{o}}(t)$, is the perimeter of the rectangle shown in figure 10 multiplied by a unit projection out of the plane of the paper.

While $B_{\mathrm{o}}(t)$ is again independent of time, the closed part $B_{\mathrm{c}}(t)$, defined as the circumference of the cylinder $x^2 + (y \pm \chi(t))^2 = R^2$, is clearly a function of time. The open control volume $R_{\mathrm{o}}(t)$ is also a function of time since its shape, though not its volume, is changing as the cylinder moves. The CV and CS definitions are illustrated in figure 10. The uniform free-stream velocity is again denoted as U_{o}. The presentation in this section highlights the derivation of the structural equation of motion and the corresponding boundary conditions on $B_{\mathrm{c}}(t)$. Derivations involving the fluid field, which are identical to those presented of §6*b*, are simply presented in final form.

In this problem, $(\mathcal{K})_{\mathrm{o}} = (\mathcal{K}_{\mathrm{fluid}} + \mathcal{K}_{\mathrm{cyl}})_{\mathrm{o}}$ and $(\mathcal{E})_{\mathrm{o}} = (\mathcal{E}^{(\mathrm{s})}_{\mathrm{cyl}})_{\mathrm{o}}$, with $(\mathcal{K}_{\mathrm{fluid}})_{\mathrm{o}}$ given by equation (6.4),

$$(\mathcal{K}_{\mathrm{cyl}})_{\mathrm{o}} = \frac{1}{2} m_{\mathrm{c}} \dot{\chi}^2 \quad \text{and} \quad \left(\mathcal{E}^{(\mathrm{s})}_{\mathrm{cyl}}\right)_{\mathrm{o}} = \frac{1}{2} k_{\mathrm{s}}^{(\chi)} \chi^2.$$

It follows that

$$(\mathcal{L})_{\mathrm{o}} = \int\int\int_{R_{\mathrm{o}}(t)} \frac{1}{2} \rho(\boldsymbol{u}\cdot\boldsymbol{u}) \mathrm{d}v + \frac{1}{2} m_{\mathrm{c}} \dot{\chi}^2 - \frac{1}{2} k_{\mathrm{s}}^{(\chi)} \chi^2. \tag{7.1}$$

Using equation (7.1), equation (6.1) becomes

$$\delta \int_{t_1}^{t_2} \int\int\int_{R_{\mathrm{o}}(t)} \frac{1}{2} \rho(\boldsymbol{u}\cdot\boldsymbol{u}) \mathrm{d}v \, \mathrm{d}t + \delta \int_{t_1}^{t_2} \frac{1}{2} m_{\mathrm{c}} \dot{\chi}^2 \, \mathrm{d}t - \delta \int_{t_1}^{t_2} \frac{1}{2} k_{\mathrm{s}}^{(y)} \chi^2 \, \mathrm{d}t$$
$$- \int_{t_1}^{t_2} \int\int\int_{R_{\mathrm{o}}(t)} \sigma_{ij} \delta\varepsilon_{ij} \, \mathrm{d}v \, \mathrm{d}t + \int_{t_1}^{t_2} \int\int_{B_{\mathrm{o}}(t)} \rho(\boldsymbol{u}\cdot\delta\boldsymbol{r})(\boldsymbol{u}\cdot\boldsymbol{n}) \mathrm{d}s \, \mathrm{d}t = 0. \tag{7.2}$$

The variation of the first term of equation (2.4) is obtained directly from equation (6.19). The variation of the second and third terms is

$$\delta\left(\mathcal{K}_{\mathrm{cyl}}\right)_{\mathrm{o}} = m_{\mathrm{c}} \dot{\chi} \delta\dot{\chi} \quad \text{and} \quad \delta\left(\mathcal{E}^{(s)}_{\mathrm{cyl}}\right)_{\mathrm{o}} = k_{\mathrm{s}}^{(\chi)} \chi \delta\chi,$$

respectively. Integration by parts, with $\delta\boldsymbol{r}(t_1) = \delta\boldsymbol{r}(t_2) = \boldsymbol{0}$ and $\delta\chi(t_1) = \delta\chi(t_2) = 0$,

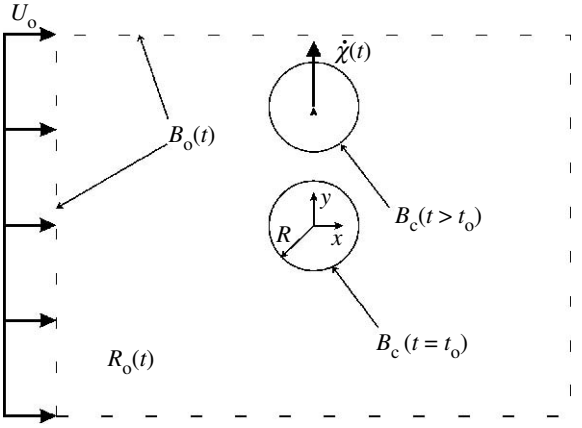

Figure 10. The open control surface $B_o(t)$, closed control surface $B_c(t)$ (at two different instances) and the open control volume $R_o(t)$ for the case of a rigid circular cylinder of radius R with 1 d.f. The cylinder is free to move transversely to the uniform incoming flow of velocity U_o. The transverse generalized coordinate is $\chi(t)$. The restraining springs are not shown.

yields

$$-\int_{t_1}^{t_2}\iiint_{R_o(t)}\rho\left(\frac{\mathrm{D}u_i}{\mathrm{D}t}\delta r_i\right)\mathrm{d}v\,\mathrm{d}t-\int_{t_1}^{t_2}m_c\ddot{\chi}\delta\chi\,\mathrm{d}t-\int_{t_1}^{t_2}k_s^{(y)}\chi\delta\chi\,\mathrm{d}t$$
$$+\int_{t_1}^{t_2}\iiint_{R_o(t)}\left[\frac{\partial\sigma_{ij}}{\partial x_j}\delta r_i\right]\mathrm{d}v\,\mathrm{d}t-\int_{t_1}^{t_2}\iint_{B_o(t)}\sigma_{ij}n_j\delta r_i\,\mathrm{d}s\,\mathrm{d}t$$
$$-\int_{t_1}^{t_2}\iint_{B_c(t)}\sigma_{ij}n_j\delta r_i\,\mathrm{d}s\,\mathrm{d}t+\int_{t_1}^{t_2}\iint_{B_o(t)}\rho u_i\delta r_i u_j n_j\,\mathrm{d}s\,\mathrm{d}t=0. \tag{7.3}$$

In arriving at equation (7.3), equations (6.20) and (6.24) are used.

Collecting like terms yields

$$-\int_{t_1}^{t_2}\iiint_{R_o(t)}\left[\rho\frac{\mathrm{D}u_i}{\mathrm{D}t}-\frac{\partial\sigma_{ij}}{\partial x_j}\right]\delta r_i\,\mathrm{d}v\,\mathrm{d}t-\int_{t_1}^{t_2}(m_c\ddot{\chi}+k_s^{(\chi)}\chi)\delta\chi\,\mathrm{d}t$$
$$+\int_{t_1}^{t_2}\iint_{B_o(t)}\left[\rho u_i u_j n_j-\sigma_{ij}n_j\right]\delta r_i\,\mathrm{d}s\,\mathrm{d}t-\int_{t_1}^{t_2}\iint_{B_c(t)}\sigma_{ij}n_j\delta r_i\,\mathrm{d}s\,\mathrm{d}t=0, \tag{7.4}$$

where δ_{2i} is the Kronecker delta function. The no-slip condition on the surface of the cylinder, together with the kinematic boundary condition ensuring that the normal components of the velocity are conserved across the fluid–structure interface, which is the no-through flow condition in the case of a solid boundary, require that $\boldsymbol{u}=\boldsymbol{V}.\boldsymbol{V}=(0,\dot{\chi})$ is the velocity vector of the cylinder. This condition implies that $\delta r_1=0$ and $\delta r_2=\chi$ on $B_c(t)$ at all times t. Furthermore, these virtual displacements hold on all points on the cylinder. The last term in

equation (2.4) can then be written as

$$\int_{t_1}^{t_2}\int\int_{B_c(t)}\sigma_{ij}n_j\delta r_i\,\mathrm{d}s\,\mathrm{d}t=\int_{t_1}^{t_2}\delta\chi\left(\int\int_{B_c(t)}\sigma_{2j}n_j\,\mathrm{d}s\right)\mathrm{d}t.$$

It follows that equation (2.4) can be rewritten as

$$-\int_{t_1}^{t_2}\int\int\int_{R_o(t)}\left[\rho\frac{\mathrm{D}u_i}{\mathrm{D}t}-\frac{\partial\sigma_{ij}}{\partial x_j}\right]\delta r_i\,\mathrm{d}v\,\mathrm{d}t-\int_{t_1}^{t_2}\left(m_c\ddot{\chi}+k_s^{(y)}\chi+\int\int_{B_c(t)}\sigma_{2j}n_j\,\mathrm{d}s\right)\delta\chi\,\mathrm{d}t$$
$$+\int_{t_1}^{t_2}\int\int_{B_o(t)}[\rho u_iu_jn_j-\sigma_{ij}n_j]\delta r_i\,\mathrm{d}s\,\mathrm{d}t=0.$$

The arbitrariness of the variations δr_i in $R_o(t)\times[t_1,t_2]$ leads to the Euler–Lagrange equations for the fluid,

$$\rho\frac{\mathrm{D}u_i}{\mathrm{D}t}=\frac{\partial\sigma_{ij}}{\partial x_j}\quad\text{in}\quad R_o(t).\tag{7.5}$$

Likewise, the variations $\delta\chi$ are arbitrary $\forall\boldsymbol{x}\in x^2+(y\pm\chi)^2\le R^2$ and for all times $[t_1,t_2]$, and this argument leads to the equation of motion of the cylinder,

$$m_c\ddot{\chi}+k_s^{(\chi)}\chi=-\int\int_{B_c(t)}\sigma_{2j}n_j\,\mathrm{d}s.\tag{7.6}$$

A similar argument regarding the variations δr_i on $B_o(t)\times[t_1,t_2]$ leads to the natural boundary condition

$$[\sigma_{ij}n_j-\rho u_iu_jn_j]\delta r_i=0\quad\text{on}\quad B_o(t).\tag{7.7}$$

The assumption of incompressibility and the corresponding constitutive relation, equation (6.35), leads to the following form of equation (7.5):

$$\rho\left(\frac{\partial u_i}{\partial t}+u_j\frac{\partial u_i}{\partial x_j}\right)=-\frac{\partial p}{\partial x_i}+\mu\frac{\partial^2u_i}{\partial x_jx_j}\quad\text{in}\quad R_o(t).\tag{7.8}$$

Equation (7.8) must be solved in conjunction with equation (7.6), the continuity equation, and the boundary condition is manifested in equation (7.7) (with $\sigma_{ij}\to\hat{\sigma}_{ij}$). This boundary condition is interpreted as $[\hat{\sigma}_{ij}n_j-\rho u_iu_jn_j]=0$ since the fluid displacements are not prescribed on $B_o(t)$. The fluid drives the cylinder with a force

$$F_2(t)=-\int\int_{B_c(t)}\hat{\sigma}_{2j}n_j\,\mathrm{d}s.$$

8. Applications to reduced-order modelling

Consider equation (2.4) with an additional term representing the work done by the structural damping force (i.e. that which changes vibrational energy into heat)

$$\overbrace{\delta\int_{t_1}^{t_2}\iiint_{R_o(t)}\frac{1}{2}\rho(\boldsymbol{u}\cdot\boldsymbol{u})\mathrm{d}v\,\mathrm{d}t}^{1}+\delta\int_{t_1}^{t_2}\frac{1}{2}m_c\dot{\chi}^2\,\mathrm{d}t$$
$$-\delta\int_{t_1}^{t_2}\frac{1}{2}k_s^{(y)}\chi^2\,\mathrm{d}t-\int_{t_1}^{t_2}c^{(\mathrm{vac})}\dot{\chi}\delta\chi\,\mathrm{d}t-\overbrace{\int_{t_1}^{t_2}\iiint_{R_o(t)}\hat{\sigma}_{ij}\left[\frac{\partial(\delta r_i)}{\partial x_j}\right]\mathrm{d}v\,\mathrm{d}t}^{2}$$
$$+\overbrace{\int_{t_1}^{t_2}\iint_{B_o(t)}\rho(\boldsymbol{u}\cdot\delta\boldsymbol{r})(\boldsymbol{u}\cdot\boldsymbol{n})\mathrm{d}s\,\mathrm{d}t}^{3}=0. \tag{8.1}$$

$c^{(\mathrm{vac})}>0$ is the linear material damping coefficient measured *in vacuo*. The structural damping force is always opposed to the velocity, such that the non-conservative virtual work, $(\delta W_{\mathrm{cyl}})_o=c^{(\mathrm{vac})}\dot{\chi}\delta\chi$, is always negative for positive $\dot{\chi}$.

In order to reduce the complexity of equation (8.1), the control volume $R_o(t)$ is first reduced to small rectangular region R^{**} incorporating the formation region. The negative damping condition initiating the cylinder motion, as well as the periodic wake feeding the growing amplitudes of the cylinder are generated in the formation region. The existence of a temporal global wake instability in the formation region allows a second, more crucial simplification to be made: the flow in R^{**} is assumed to be represented by the representative mass m_{fl} whose transverse displacement is $w(t)$. All spatial dependencies are lost.

It emphasized that while $\dot{w}(t)$ and $\dot{\chi}(t)$ ($\ddot{w}(t)$ and $\ddot{\chi}(t)$) are both transverse velocities (accelerations), they need not always have the same sign at any one instant. It is therefore important to talk about *relative* velocities (accelerations).

Term '1' of equation (8.1) is reduced to

$$\delta\int_{t_1}^{t_2}\iiint_{R_o(t)}\frac{1}{2}\rho(\boldsymbol{u}\cdot\boldsymbol{u})\mathrm{d}v\,\mathrm{d}t\Rightarrow\int_{t_1}^{t_2}\hat{a}_0 m_{\mathrm{fl}}\ddot{w}\delta\dot{w}\,\mathrm{d}t, \tag{8.2}$$

where $\hat{a}_0$ is a dimensionless constant. Term '2' can likewise be reduced. Term '3' is eliminated because the energy fed through the vertical face fore (upstream) of the cylinder only *indirectly* contributes to near-wake dynamics by providing the energy for the development of the wake flow. The face aft (downstream) of the cylinder is no longer involved in the near-wake mechanics.

Suppose the following separation is made:

$$-\int_{t_1}^{t_2}\hat{\sigma}_{ij}\left[\frac{\partial(\delta r_i)}{\partial x_j}\right]\mathrm{d}v\,\mathrm{d}t\Rightarrow-\int_{t_1}^{t_2}\delta W(w,\dot{w},\ddot{w},\chi,\dot{\chi},\ddot{\chi},t)\mathrm{d}t-\int_{t_1}^{t_2}F(w,t)\delta w\,\mathrm{d}t. \tag{8.3}$$

The functional $F(w,t)=\hat{a}_1 m_{\mathrm{fl}} f_{\mathrm{st}} U_o w(t)/D$ represents the 'fluid stiffness' term, where $\hat{a}_1$ is a dimensionless constant and $f_{\mathrm{st}}=SU/D$ is the vortex shedding or Strouhal frequency of the cylinder when it is stationary ($S\sim 0.2$ is the Strouhal number). The coefficient $\hat{a}_1 m_{\mathrm{fl}} f_{\mathrm{st}} U_o/D$ represents the natural frequency of the undamped wake oscillator for small $w(t)$ (no motion of the cylinder), and is

consistent with the observation that the damped (and hence the undamped) natural frequency of the wake oscillator must change as the flow velocity U_o changes (Billah 1989).

The fundamental character of a wake oscillator model is that when it is uncoupled from the cylinder motion, it has a definite natural frequency

$$(\hat{a}_1 m_{fl} f_{st} U_o/D)^{0.5},$$

which changes when U_o changes.

Using equations (8.2) and (8.3), equation (8.1) becomes

$$\int_{t_1}^{t_2} \hat{a}_0 m_{fl} \dot{w}\delta\dot{w}\,dt + \delta\int_{t_1}^{t_2} \frac{1}{2} m_c \dot{\chi}^2\,dt - \delta\int_{t_1}^{t_2} \frac{1}{2} k_s^{(y)} \chi^2\,dt - \int_{t_1}^{t_2} c^{(vac)}\dot{\chi}\delta\chi\,dt$$
$$- \int_{t_1}^{t_2} \delta W(w, \dot{w}, \ddot{w}, \chi, \dot{\chi}, \ddot{\chi}, t)\,dt - \int_{t_1}^{t_2} F(w,t)\delta w\,dt = 0. \tag{8.4}$$

Next, consider dividing the functional $\delta W(w, \dot{w}, \ddot{w}, \chi, \dot{\chi}, \ddot{\chi}, t)$ as follows:

$$\delta W(w, \dot{w}, \ddot{w}, \chi, \dot{\chi}, \ddot{\chi}, t) = -F_{fl/st}^{(y)}(w, \dot{w}, \ddot{w}, \chi, \dot{\chi}, \ddot{\chi}, t)\delta\chi$$
$$+ F_{\mu/p}^{(y)}(w, \dot{w}, \ddot{w}, \chi, \dot{\chi}, \ddot{\chi}, t)\delta w. \tag{8.5}$$

$F_{fl/st}^{(y)}(w, \dot{w}, \ddot{w}, \chi, \dot{\chi}, \ddot{\chi}, t)\delta\chi$ is the instantaneous virtual work done by total transverse hydrodynamic force acting on the cylinder, while $F_{\mu/p}^{(y)}(w, \dot{w}, \ddot{w}, \chi, \dot{\chi}, \ddot{\chi}, t)\delta w$ represents virtual work done by the vertical components of the viscous and pressure forces within R^{**}, excluding the boundary of the cylinder. The negative sign on the $F_{fl/st}^{(y)}(w, \dot{w}, \ddot{w}, \chi, \dot{\chi}, \ddot{\chi}, t)\delta\chi$ term is due to the fact that on the surface of the cylinder $\delta\chi = -\delta w$ owing to the no-slip condition.

Suppose the following form is assumed for $F_{fl/st}^{(y)}$:

$$F_{fl/st}^{(y)}(w, \dot{w}, \ddot{w}, \chi, \dot{\chi}, \ddot{\chi}, t) = -\frac{1}{4}\rho\pi D^2 L C_a \ddot{\chi}(t) + \frac{1}{2}\rho D L C_d[\dot{w}(t) - \dot{\chi}(t)]|\dot{w}(t) - \dot{\chi}(t)|$$
$$+ \frac{1}{4}\pi\rho D^2 L(1 + C_a)\ddot{w}(t). \tag{8.6}$$

C_a represents the time-dependent added mass coefficient for a moving cylinder in a crossflow. It is not the same as the potential flow added mass $C_A = 1$. C_d represents the component of the instantaneous vortex lift coefficient $C_L(t)$ that is out of phase with the cylinder displacement.

Note that the form of equation (8.6) is equivalent to the Morison–O'Brien–Johnson–Schaff (MOJS) equation for the fluid force on a cylinder moving parallel to a time-dependent fluid stream (Sarpkaya 2004). In principle, geometric considerations require that the MOJS equation be modified when the cylinder is moving transversely to the free stream. Here, however, equation (8.6) is retained unaltered with the understanding that said equation can then be only referred to as 'MOJS-like'.

The following form is assumed for $F_{\mu/p}(\dot{w}, \ddot{w}, \chi, \dot{\chi}, \ddot{\chi}, t)$:

$$F_{\mu/p}(\dot{w}, \ddot{w}, \chi, \dot{\chi}, \ddot{\chi}, t) = \hat{a}_2 m_{\mathrm{fl}} f_{\mathrm{st}} [\dot{w}(t) - \dot{\chi}(t)] + \frac{\hat{a}_3 m_{\mathrm{fl}} f_{\mathrm{st}}}{U_{\mathrm{o}}^2} [\dot{w}(t) - \dot{\chi}(t)]^3. \tag{8.7}$$

The $\hat{a}_i$'s are again dimensionless constants.

The functional $F_{\mu/p}(w, \dot{w}, \ddot{w}, \chi, \dot{\chi}, \ddot{\chi}, t)$ has two distinct roles. In the first place, it is intended to capture the nonlinear damping effects in the wake oscillator, much like the $\varepsilon f_{\mathrm{st}}(\dot{q}^2(t) - 1)\dot{q}(t)$ term in the Rayleigh equation, or the $\varepsilon f_{\mathrm{st}}(q^2(t) - 1)\dot{q}(t)$ term in the van der Pol equation. This damping term must be such that the wake oscillator is self-excited and self-limiting.

Self-excitation of the wake is due to amplification by the shear layers of initial instabilities generated at the separation points, and an upstream influence caused by a region of absolute instability in the near wake. This region of absolute instability, whose downstream boundary is the point in the wake where travelling waves can be reflected, is associated with causing the propagation an upstream travelling wave disturbance which amounts to a 'feedback' to the separation points.

In addition, $F_{\mu/p}(\dot{w}, \ddot{w}, \chi, \dot{\chi}, \ddot{\chi}, t)$ must represent the nonlinear interaction (i.e. r.h.s.) between the wake oscillator and the motion of the cylinder.

First, equations (8.6) and (8.7) are substituted in equation (8.5). The result is then replaced in equation (8.4), and the indicated variations performed. The conditions $\delta w\big|_{t_1}^{t_2} = \delta\chi\big|_{t_1}^{t_2} = 0$ are imposed and similar terms collected. The independence of the variations $\delta\chi$ and δw leads to the following set of coupled differential equations:

$$\begin{aligned}&\left(m_{\mathrm{c}} + \frac{1}{4}\pi\rho D^2 L C_{\mathrm{a}}\right)\ddot{\chi}(t) + c^{(\mathrm{vac})}\dot{\chi}(t) + k_{\mathrm{s}}^{(\chi)}\chi(t)\\ &\quad = \frac{1}{2}\rho D L C_{\mathrm{d}} |\dot{w}(t) - \dot{\chi}(t)| [\dot{w}(t) - \dot{\chi}(t)] + \frac{1}{4}\pi\rho D^2 L (C_{\mathrm{a}} + 1)\ddot{w}(t)\end{aligned} \tag{8.8}$$

and

$$\begin{aligned}&\hat{a}_0 m_{\mathrm{fl}} \ddot{w}(t) + \hat{a}_1 m_{\mathrm{fl}} \frac{U_{\mathrm{o}} f_{\mathrm{st}}}{D} w(t) + \frac{m_{\mathrm{fl}} f_{\mathrm{st}}}{U_{\mathrm{o}}^2} \left[\hat{a}_3 \dot{w}^2(t) + \hat{a}_2 U_{\mathrm{o}}^2\right] \dot{w}(t)\\ &\quad = \hat{a}_2 m_{\mathrm{fl}} f_{\mathrm{st}} \dot{\chi}(t) + \frac{\hat{a}_3 m_{\mathrm{fl}} f_{\mathrm{st}}}{U_{\mathrm{o}}^2} \dot{\chi}^3(t) + \frac{3\hat{a}_3 m_{\mathrm{fl}} f_{\mathrm{st}}}{U_{\mathrm{o}}^2} [\dot{w}^2(t)\dot{\chi}(t) - \dot{w}(t)\dot{\chi}^2(t)].\end{aligned} \tag{8.9}$$

9. Comparison with other wake oscillator models

Equations (8.8) and (8.9) are obtained as a reduced-order model for the self-excited transverse motion of an elastically mounted rigid circular cylinder in a smooth flow. The displacement of the cylinder from equilibrium, $\chi(t)$, is governed by equation (8.8). The fluctuating lift force resulting from vortex shedding acts as the primary driving force. Again, the fluctuating lift force is assumed to be correlated along the entire span.

The forcing function on r.h.s. of equation (8.8) is a function of both the relative transverse velocity and the acceleration of the representative fluid mass m_{fl}. Recall that the transverse displacement of this fluid mass from the cylinder's horizontal (x) line of symmetry is denoted $w(t)$. For a stationary cylinder, the

displacement is denoted $w_o(t)$. The fluid d.f. $w(t)$ represents the mean transverse displacement of the collection of fluid particles having a total mass m_{fl} at each time t.

First, define the dimensionless displacement variables

$$\Xi(t) = \frac{\chi(t)}{D} \quad \text{and} \quad W(t) = \frac{w(t)}{D}$$

and the dimensionless time variable

$$T = t\omega_{st},$$

where $\omega_{st} = 2\pi f_{st}$ is the circular Strouhal frequency.

(a) *The structural oscillator*

Using the above-transformed variables, equation (8.8) becomes

$$(m_c + m_d C_a)\Xi''(T) + \frac{c^{(vac)}}{\omega_{st}}\Xi'(T) + \frac{k_s^{(y)}}{\omega_{st}^2}\Xi(T)$$

$$= \frac{1}{2}\rho D^2 L C_d |W'(T) - \Xi'(T)|[W'(T) - \Xi'(T)] + m_d(1 + C_a)W''(T), \quad (9.1)$$

where $m_d = \rho\pi D^2 L/4$.

Next, we define the *in vacuo* natural frequency,

$$\omega_n^{(vac)} = \sqrt{\frac{k_s^{(y)}}{m_c}} \simeq \omega_n^{(air)} \quad (9.2)$$

and the *in situ* (Skop & Balasubramanian 1997) or *true* (Vikestad *et al.* 2000) natural frequency of the cylinder in crossflow,

$$\omega_n^{(true)} = \sqrt{\frac{k_s^{(y)}}{(m_c + m_d C_a)}}, \quad (9.3)$$

where $m_d C_a = \rho\pi D^2 L C_a/4 \equiv \Delta m$ is the added mass.

The identity

$$\Delta m = m_d C_a = m_c\left[\left(\frac{\omega_n^{(vac)}}{\omega_n^{(true)}}\right)^2 - 1\right] \quad (9.4)$$

is readily verified via equations (9.2) and (9.3). Using this identity, the virtual mass can be expressed as

$$(m_c + \Delta m) = (m_c + m_d C_a) = m_c\left(\frac{\omega_n^{(vac)}}{\omega_n^{(true)}}\right)^2. \quad (9.5)$$

Substituting equation (9.5) in equation (9.1) yields

$$\Xi''(T)+\frac{1}{\omega_{\mathrm{st}}}\left(\frac{\omega_{\mathrm{n}}^{(\mathrm{true})}}{\omega_{\mathrm{n}}^{(\mathrm{vac})}}\right)^2\frac{c^{(\mathrm{vac})}}{m_{\mathrm{c}}}\Xi'(T)+\frac{1}{\omega_{\mathrm{st}}^2}\left(\frac{\omega_{\mathrm{n}}^{(\mathrm{true})}}{\omega_{\mathrm{n}}^{(\mathrm{vac})}}\right)^2\frac{k_{\mathrm{s}}^{(y)}}{m_{\mathrm{c}}}\Xi(T)$$

$$=\frac{1}{2m_{\mathrm{c}}}\left(\frac{\omega_{\mathrm{n}}^{(\mathrm{true})}}{\omega_{\mathrm{n}}^{(\mathrm{vac})}}\right)^2\rho D^2LC_{\mathrm{d}}|W'(T)-\Xi'(T)|\big[W'(T)-\Xi'(T)\big]$$

$$+\frac{m_{\mathrm{d}}}{m_{\mathrm{c}}}\left(\frac{\omega_{\mathrm{n}}^{(\mathrm{true})}}{\omega_{\mathrm{n}}^{(\mathrm{vac})}}\right)^2(1+C_{\mathrm{a}})W''(T). \tag{9.6}$$

Introducing the reduced mass

$$\hat{m}^*=\frac{\rho\pi D^2L}{4m_{\mathrm{c}}}=\frac{m_{\mathrm{d}}}{m_{\mathrm{c}}} \tag{9.7}$$

and the *in vacuo* structural damping ratio

$$\zeta^{(\mathrm{vac})}=\frac{c^{(\mathrm{vac})}}{2m_{\mathrm{c}}\omega_{\mathrm{n}}^{(\mathrm{vac})}} \tag{9.8}$$

into equation (9.6) and using equation (9.2) yields

$$\Xi''(T)+\frac{2}{\omega_{\mathrm{st}}}\left(\frac{\omega_{\mathrm{n}}^{(\mathrm{true})}}{\omega_{\mathrm{n}}^{(\mathrm{vac})}}\right)^2\zeta^{(\mathrm{vac})}\omega_{\mathrm{n}}^{(\mathrm{vac})}\Xi'(T)+\frac{1}{\omega_{\mathrm{st}}^2}\left(\frac{\omega_{\mathrm{n}}^{(\mathrm{true})}}{\omega_{\mathrm{n}}^{(\mathrm{vac})}}\right)^2{\omega_{\mathrm{n}}^{(\mathrm{vac})}}^2\Xi(T)$$

$$=\frac{2}{\pi}\left(\frac{\omega_{\mathrm{n}}^{(\mathrm{true})}}{\omega_{\mathrm{n}}^{(\mathrm{vac})}}\right)^2\hat{m}^*C_{\mathrm{d}}|W'(T)-\Xi'(T)|[W'(T)-\Xi'(T)]$$

$$+\hat{m}^*\left(\frac{\omega_{\mathrm{n}}^{(\mathrm{true})}}{\omega_{\mathrm{n}}^{(\mathrm{vac})}}\right)^2(1+C_{\mathrm{a}})W''(T). \tag{9.9}$$

By rearranging equation (9.4) and using equation (9.7), the useful identity

$$\left(\frac{\omega_{\mathrm{n}}^{(\mathrm{true})}}{\omega_{\mathrm{n}}^{(\mathrm{vac})}}\right)^2=\frac{1}{(1+\hat{m}^*C_{\mathrm{a}})} \tag{9.10}$$

is obtained.

Suppose the mass ratio

$$\mu=\frac{\rho\pi D^2L}{4(m_{\mathrm{c}}+\Delta m)}=\frac{\rho\pi D^2L}{4(m_{\mathrm{c}}+m_{\mathrm{d}}C_{\mathrm{a}})}=\frac{m_{\mathrm{d}}}{(m_{\mathrm{c}}+m_{\mathrm{d}}C_{\mathrm{a}})} \tag{9.11}$$

is now introduced. Note that there exists the following relationship between $\hat{m}^*$, defined by equation (9.7), and μ:

$$\mu=\frac{m_{\mathrm{d}}}{(m_{\mathrm{c}}+m_{\mathrm{d}}C_{\mathrm{a}})}=\frac{m_{\mathrm{d}}}{m_{\mathrm{c}}}\left[\frac{1}{(1+\hat{m}^*C_{\mathrm{a}})}\right]=\frac{\hat{m}^*}{(1+\hat{m}^*C_{\mathrm{a}})}. \tag{9.12}$$

The *corrected* structural damping (Skop & Balasubramanian 1997) is defined as

$$\zeta^{(\mathrm{true})} = \zeta^{(\mathrm{vac})}\sqrt{\frac{1}{(1+\hat{m}^* C_\mathrm{a})}}. \tag{9.13}$$

From equations (9.10) and (9.13), the identity

$$\begin{aligned}\left(\frac{\omega_\mathrm{n}^{(\mathrm{true})}}{\omega_\mathrm{n}^{(\mathrm{vac})}}\right)^2\zeta^{(\mathrm{vac})} &= \left(\frac{\omega_\mathrm{n}^{(\mathrm{true})}}{\omega_\mathrm{n}^{(\mathrm{vac})}}\right)\left(\frac{\omega_\mathrm{n}^{(\mathrm{true})}}{\omega_\mathrm{n}^{(\mathrm{vac})}}\right)\zeta^{(\mathrm{vac})}\\ &= \left(\sqrt{\frac{1}{1+\hat{m}^* C_\mathrm{a}}}\zeta^{(\mathrm{vac})}\right)\left(\frac{\omega_\mathrm{n}^{(\mathrm{true})}}{\omega_\mathrm{n}^{(\mathrm{vac})}}\right) = \left(\frac{\omega_\mathrm{n}^{(\mathrm{true})}}{\omega_\mathrm{n}^{(\mathrm{vac})}}\right)\zeta^{(\mathrm{true})}\end{aligned} \tag{9.14}$$

is established.

Using equations (9.13) and (9.14) in equation (9.9) leads to

$$\begin{aligned}&\Xi''(T) + 2\zeta^{(\mathrm{true})}\left(\frac{\omega_\mathrm{n}^{(\mathrm{true})}}{\omega_\mathrm{st}}\right)\Xi'(T) + \left(\frac{\omega_\mathrm{n}^{(\mathrm{true})}}{\omega_\mathrm{st}}\right)^2\Xi(T)\\ &\quad= \frac{2}{\pi}\,\frac{\hat{m}^*}{(1+\hat{m}^* C_\mathrm{a})}\,C_\mathrm{d}|\,W'(T)-\Xi'(T)|[\,W'(T)-\Xi'(T)]\\ &\qquad+\frac{\hat{m}^*}{(1+\hat{m}^* C_\mathrm{a})}(1+C_\mathrm{a})\,W''(T).\end{aligned} \tag{9.15}$$

Finally, using equation (9.12), equation (9.15) can be rewritten as

$$\begin{aligned}&\Xi''(T) + 2\zeta^{(\mathrm{true})}\left(\frac{\omega_\mathrm{n}^{(\mathrm{true})}}{\omega_\mathrm{st}}\right)\Xi'(T) + \left(\frac{\omega_\mathrm{n}^{(\mathrm{true})}}{\omega_\mathrm{st}}\right)^2\Xi(T)\\ &\quad= \frac{2}{\pi}\,\mu C_\mathrm{d}|\,W'(T)-\Xi'(T)|[\,W'(T)-\Xi'(T)] + \mu(1+C_\mathrm{a})\,W''(T).\end{aligned} \tag{9.16}$$

(*b*) *The wake oscillator*

Introducing the dimensionless variables $(\Xi, \Xi', \Xi'', W, W', W'', T)$ into equation (8.9) and rearranging gives

$$\begin{aligned}&\hat{a}_0\omega_\mathrm{st}^2 D\,W''(T) + \frac{\omega_\mathrm{st}}{U_\mathrm{o}^2}\left[\hat{a}_3 D^2\omega_\mathrm{st}^2\,W'^2(T) + \hat{a}_2\,U_\mathrm{o}^2\right]D\omega_\mathrm{st}\,W'(T) + \frac{\hat{a}_1\omega_\mathrm{st}\,U_\mathrm{o}}{D}\,DW(T)\\ &\quad= -\frac{3\hat{a}_4\omega_\mathrm{st}}{U_\mathrm{o}^2}\,D^3\omega_\mathrm{st}^3\left[W'(t)\Xi'^2(T) - \Xi'(T)\,W'^2(T)\right] + \frac{\hat{a}_3\omega_\mathrm{st}^4 D^3}{U_\mathrm{o}^2}\,\Xi'^3(T)\\ &\qquad+\hat{a}_2 D\omega_\mathrm{st}^2\Xi'(T).\end{aligned} \tag{9.17}$$

Dividing both sides of equation (9.17) by $\hat{a}_0\omega_{\mathrm{st}}^2 D$ yields[2]

$$W''(T)+\frac{\omega_{\mathrm{st}}}{U_{\mathrm{o}}^2}\left[D^2\omega_{\mathrm{st}}\frac{\hat{a}_3}{\hat{a}_0}W'^2(T)+\frac{U_{\mathrm{o}}^2}{\omega_{\mathrm{st}}}\frac{\hat{a}_2}{\hat{a}_0}\right]W'(T)+\frac{U_{\mathrm{o}}}{D\omega_{\mathrm{st}}}\frac{\hat{a}_1}{\hat{a}_0}W(T)$$
$$=-\frac{3D^2\omega_{\mathrm{st}}^2}{U_{\mathrm{o}}^2}\frac{\hat{a}_4}{\hat{a}_0}\left[W'(t)\Xi'^2(T)-\Xi'(T)W'^2(T)\right]+\frac{D^2\omega_{\mathrm{st}}^2}{U_{\mathrm{o}}^2}\frac{\hat{a}_3}{\hat{a}_0}\Xi'^3(T)+\frac{\hat{a}_2}{\hat{a}_0}\Xi'(T). \tag{9.18}$$

Noting that from the definition of the Strouhal frequency,

$$\frac{U_{\mathrm{o}}}{D\omega_{\mathrm{st}}}=\frac{U_{\mathrm{o}}}{D\left(\frac{2\pi SU_{\mathrm{o}}}{D}\right)}=\frac{1}{(2\pi S)},$$

equation (9.18) can be rewritten as

$$W''(T)\left[(2\pi S)^2\frac{\hat{a}_3}{\hat{a}_0}W'^2(T)+\frac{\hat{a}_2}{\hat{a}_0}\right]W'(T)+\frac{1}{(2\pi S)}\frac{\hat{a}_1}{\hat{a}_0}W(T)$$
$$=-3(2\pi S)^2\frac{\hat{a}_4}{\hat{a}_0}\left[W'(T)\Xi'^2(T)-\Xi'(T)W'^2(T)\right]+(2\pi S)^2\frac{\hat{a}_3}{\hat{a}_0}\Xi'^3(T)+\frac{\hat{a}_2}{\hat{a}_0}\Xi'(T). \tag{9.19}$$

Consider for the moment the case of a stationary cylinder. In this case, $\Xi(T)$ and its derivatives are all identically 0, and equation (9.19) reduces to

$$W_{\mathrm{o}}''(T)+\left[(2\pi S)^2\frac{\hat{a}_3}{\hat{a}_0}W_{\mathrm{o}}'^2(T)+\frac{\hat{a}_2}{\hat{a}_0}\right]W_{\mathrm{o}}'(T)+\frac{1}{(2\pi S)}\frac{\hat{a}_1}{\hat{a}_0}W_{\mathrm{o}}(T)=0, \tag{9.20}$$

where

$$W_{\mathrm{o}}(T)=\frac{w_{\mathrm{o}}(T)}{D}.$$

The van der Pol and Rayleigh equations are the nonlinear oscillators most commonly used to model the fluctuating nature of the vortex shedding. For a stationary cylinder, they adequately model the self-sustained, quasi-harmonic oscillations seen experimentally in the lift coefficient, for example. The reader is referred to Facchinetti *et al.* (2004) for a more comprehensive discussion. Here, the focus is on constructing a Rayleigh-type equation from equation (9.20).

The dimensionless Rayleigh equation,

$$Q''(T)+\varepsilon(Q'^2(T)-1)Q'(T)+Q(T)=0,$$

with $0<\varepsilon\ll 1$, is known to provide a stable quasi-harmonic oscillation of finite amplitude at the frequency

$$\Omega=1.$$

[2] The model constant $\hat{a}_0$ is assumed to be non-zero at all times.

Equation (9.20) is then of the Rayleigh type provided that the conditions

$$\frac{1}{(2\pi S)}\frac{\hat{a}_1}{\hat{a}_0}=1,\quad \frac{\hat{a}_2}{\hat{a}_0}<0,\quad \left|\frac{\hat{a}_2}{\hat{a}_0}\right|\ll 1,\quad \frac{\hat{a}_3}{\hat{a}_0}<0\quad \text{and}\quad (2\pi S)^2\left|\frac{\hat{a}_3}{\hat{a}_0}\right|\ll 1$$

are satisfied. It is evident from the above conditions that if $\hat{a}_0<0$, then $\hat{a}_2>0$ and $\hat{a}_{1,3}<0$. On the other hand, if $\hat{a}_0>0$, then $\hat{a}_2<0$ and $\hat{a}_{1,3}>0$.

Next, define

$$\hat{b}_i=\left|\frac{\hat{a}_i}{\hat{a}_0}\right|,$$

where $i=2,\ 3$. The sign of the model constant $\hat{a}_4$ is not known *a priori* and, therefore, there are no constraints to determine the sign of the ratio $\hat{a}_4/\hat{a}_0$. As a result, said ratio is represented as b_4, where $b_4\lessgtr 0$.

Equation (9.19) can now be written as

$$W''(T)+\left[(2\pi S)^2\hat{b}_3W'^2(T)-\hat{b}_2\right]W'(T)+W(T)$$
$$=-3(2\pi S)^2b_4\left[W'(T)\Xi'^2(T)-\Xi'(T)W'^2(T)\right]+(2\pi S)^2\hat{b}_3\Xi'^3(T)-\hat{b}_2\Xi'(T). \tag{9.21}$$

Upon examining equations (9.16) and (9.21), it is apparent that there are five model parameters $(\hat{b}_2, \hat{b}_3, b_4, C_\mathrm{a}, C_\mathrm{d})$. However, since $\hat{b}_2$, $\hat{b}_3$ and b_4 are not all independent, the true number of independent model parameters is actually six $(\hat{a}_0, \hat{a}_2, \hat{a}_3, \hat{a}_4, C_\mathrm{a}, C_\mathrm{d})$.

(*c*) *Comparison with the model of Krenk & Nielsen (1999)*

In dimensionless form, the model equations derived by Krenk & Nielsen (KN; Krenk & Nielsen 1999) are given by

$$\ddot{\Xi}(t)+\zeta^{(\mathrm{true})}\omega_\mathrm{n}^{(\mathrm{true})}\dot{\Xi}(t)+\left[\omega_\mathrm{n}^{(\mathrm{true})}\right]^2\Xi(t)=\mu_\mathrm{f}c_\mathrm{o}\omega_\mathrm{st}\dot{P}(t) \tag{9.22}$$

and

$$\ddot{P}(t)+2\zeta_\mathrm{f}\omega_\mathrm{st}\left[P^2(t)+\left(\frac{\dot{P}(t)}{\omega_\mathrm{st}}\right)^2-1\right]\dot{P}(t)+\omega_\mathrm{st}^2P(t)=-\frac{1}{v_\mathrm{o}^2}c_\mathrm{o}\omega_\mathrm{st}\dot{\Xi}(t), \tag{9.23}$$

where

$$\mu_\mathrm{f}=\frac{\rho D^2L}{(m_\mathrm{c}+\Delta m)} \tag{9.24}$$

and $\zeta_\mathrm{f}\equiv$ equivalent fluid damping ratio.

It is not clear from Krenk & Nielsen (1999) how the added fluid mass, Δm in equation (9.24), is defined. Since KN test the validity of their model using data from experiments conducted in air, the added fluid mass is small. That is, for $\hat{m}^*\ll 1$, $\Delta m_\mathrm{potential}=C_\mathrm{A}\hat{m}^*m_\mathrm{c}\simeq\Delta m=C_\mathrm{a}\hat{m}^*m_\mathrm{c}\simeq 0$. Thus, the distinction between $\Delta m_\mathrm{potential}$ and Δm matters little in this case. This is not the case if the fluid medium is water.

The physical meaning of fluid variable[3] $W^*(t)$ in the KN model is also not clearly defined. It is conjectured here that this fluid variable represents the *relative* transverse displacement of the fluid mass m_{fl}. Designating this conjectured KN wake variable as $W^*_{\mathrm{conj.}}(t)$, it follows that

$$W^*_{\mathrm{conj.}}(t) = w(t) - \chi(t).$$

Krenk & Nielsen non-dimensionalize their fluid variable as follows:

$$P(t) = \frac{W^*(t)}{w_{\mathrm{o}}}.$$

As before, the scale w_{o} is a parameter that '…controls the amplitude of self-induced vibrations of the wake oscillator in the case of a stationary cylinder…' (Krenk & Nielsen 1999).

The parameters c_{o} and v_{o} of equations (9.22) and (9.23) are defined as

$$c_{\mathrm{o}} = \frac{w_{\mathrm{o}}\gamma}{4\pi SD} \tag{9.25}$$

and

$$v_{\mathrm{o}} = \frac{w_{\mathrm{o}}}{D}, \tag{9.26}$$

where γ is a dimensionless coupling parameter.

The dimensionless time variable $T = \omega_{\mathrm{st}} t$ is now introduced. Effecting the change of variables $t \rightarrow T$ in equations (9.22) and (9.23) results in

$$\Xi''(T) + \zeta^{(\mathrm{true})}\left(\frac{\omega_{\mathrm{n}}^{(\mathrm{true})}}{\omega_{\mathrm{st}}}\right)\Xi'(T) + \left(\frac{\omega_{\mathrm{n}}^{(\mathrm{true})}}{\omega_{\mathrm{st}}}\right)^2 \Xi(T) = \mu_{\mathrm{f}} c_{\mathrm{o}} P'(T) \tag{9.27}$$

and

$$P''(T) + 2\zeta_{\mathrm{f}}[P^2(T) + P'^2(T) - 1] + P(T) = -\frac{1}{v_{\mathrm{o}}^2} c_{\mathrm{o}} \Xi'(T), \tag{9.28}$$

respectively.

Comparing equations (9.11) and (9.24), it is seen that

$$\mu_{\mathrm{f}} = \frac{\rho D^2 L}{(m_{\mathrm{c}} + \Delta m)} = \frac{4}{\pi}\mu.$$

Using this result and equations (9.25) and (9.26), equations (9.27) and (9.28) can then be rewritten, respectively, as

$$\Xi''(T) + \zeta^{(\mathrm{true})}\left(\frac{\omega_{\mathrm{n}}^{(\mathrm{true})}}{\omega_{\mathrm{st}}}\right)\Xi'(T) + \left(\frac{\omega_{\mathrm{n}}^{(\mathrm{true})}}{\omega_{\mathrm{st}}}\right)^2 \Xi(T) = \frac{4 w_{\mathrm{o}}\gamma}{\pi^2 SD}\mu P'(T) \tag{9.29}$$

and

$$P''(T) + 2\zeta_{\mathrm{f}}\left[P^2(T) + P'^2(T) - 1\right]P'(T) + P(T) = -\frac{D\gamma}{4\pi S w_{\mathrm{o}}}\Xi'(T). \tag{9.30}$$

[3] The actual fluid variable that is used in the formulation of their model.

Using the definition of $W^*_{\text{conj.}}(t)$, it is possible to define the new dimensionless variable

$$P_{\text{conj.}}(T) = \frac{W^*_{\text{conj.}}(T)}{w_{\text{o}}}.$$

Its derivative is

$$P'_{\text{conj.}}(T) = \frac{W^{*\prime}_{\text{conj.}}(T)}{v_{\text{o}} D} = \frac{1}{v_{\text{o}}}\left(\frac{D W'(T) - D\Xi'(T)}{D}\right) = \frac{1}{\nu_{\text{o}}}[W'(T) - \Xi'(T)].$$

Making the substitution $P'(T) \to P'_{\text{conj.}}(T)$ on the r.h.s. of equation (9.29) yields

$$\Xi''(T) + \zeta^{(\text{true})}\left(\frac{\omega_{\text{n}}^{(\text{true})}}{\omega_{\text{st}}}\right)\Xi'(T) + \left(\frac{\omega_{\text{n}}^{(\text{true})}}{\omega_{\text{st}}}\right)^2 \Xi(T) = \frac{4w_{\text{o}}\gamma}{\pi^2 SD}\mu P'_{\text{conj.}}(T)$$
$$= \frac{4w_{\text{o}}\gamma}{\pi^2 SD}\mu[W'(T) - \Xi'(T)]. \tag{9.31}$$

Comparing equations (9.16) and (9.30), it is clear that the l.h.s. of each equation is the same. The r.h.s., on the other hand, differs. Equation (9.30) has a r.h.s. that represents a linearized form of the drag term in equation (9.16). Also absent from the r.h.s. of equation (9.30) is a term proportional to the acceleration of the representative fluid mass, $P''(T)$.

Now, suppose that $W^*_{\text{conj.}}(t) = W^*(t)$. This implies that there is no distinction between $P_{\text{conj.}}(T) = P(T)$. In this case, equation (9.27) reveals that in this case there is no *per se* fluid added damping. The structural oscillator is fed energy directly from the wake oscillator via the $\mu_{\text{f}} c_{\text{o}} P'(T)$ term on the r.h.s., but it is not possible to explicitly express the dependence of this energy transfer on the cylinder velocity $\Xi'(T)$.

Prima facie, equations (9.21) and (9.29) seem nothing alike. In the first place, equation (9.21) lacks a term of the form $W^2(T)W'(T)$, which is present in equation (9.29). Also, the r.h.s. of equation (9.29) is linearly proportional to cylinder velocity $\Xi'(T)$, while equation (9.21) possesses an additional nonlinear forcing function.

However, if $P_{\text{conj.}}(T)$ and its derivatives,

$$P_{\text{conj.}}(T) = \frac{1}{v_{\text{o}}}[W(T) - \Xi(T)],$$

$$P'_{\text{conj.}}(T) = \frac{1}{v_{\text{o}}}[W'(T) - \Xi'(T)]$$

and

$$P''_{\text{conj.}}(T) = \frac{1}{v_{\text{o}}}[W''(T) - \Xi''(T)]$$

are substituted into equation (9.29) in place of $P(T)$ and its derivatives, a complex forcing function is obtained. In fact, this expression will include all the terms on the r.h.s. of equation (9.21) plus additional nonlinear terms originating from the product

$$2\zeta_{\text{f}}\left[\left\{\frac{1}{v_{\text{o}}}[W(T) - \Xi(T)]\right\}^2\right][W'(T) - \Xi'(T)].$$

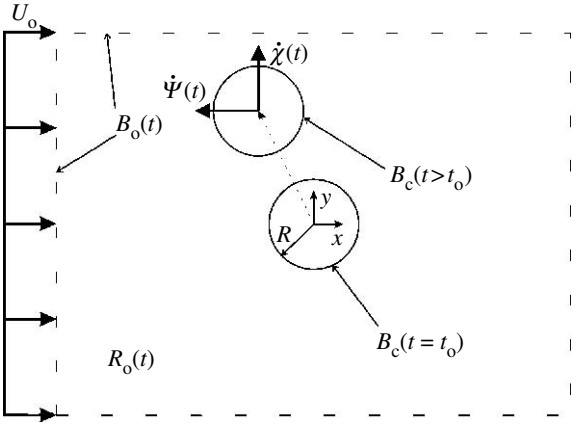

Figure 11. The open control surface $B_o(t)$, closed control surface $B_c(t)$ (at two different instances) and the open control volume $R_o(t)$ for the case of uniform flow U_o past an elastically mounted circular cylinder (radius R) with 2 d.f. The in-line and transverse generalized coordinates are $\chi(t)$ and $\Psi(t)$, respectively. The restraining springs are not shown.

Note that the forcing function will also involve terms that are linear in the cylinder displacement $\Xi(T)$, velocity $\Xi'(T)$ and acceleration $\Xi''(T)$. The $\Xi(T)$ and $\Xi''(T)$ terms are absent from equation (9.21).

It is fair to say that comparison with the KN model is complicated by uncertainty with respect to the definition of the fluid variable $W^*(t)$; very different conclusions are reached depending on how $W^*(t)$ is interpreted.

10. Concluding thoughts

One of our motivations in the studies presented here has been to better understand flow-oscillator models. By this we mean that it is important to understand the links between flow-oscillator models and first principles. In keeping with this goal, a theoretical framework for the analysis of the fluid–structure interaction problem consisting of a rigid circular cylinder in a uniform viscous flow has been presented. The method has been used to derive the relevant dynamic equations of the fully coupled interaction in two distinct cases: (i) a stationary cylinder and (ii) a cylinder with a transverse degree of freedom only. The latter was used as a model problem with which to illustrate the potential role of the proposed variational framework as a mechanism by which reduced-order models can be obtained. In particular, a class of wake oscillator models was derived, with the immediate benefit of giving these types of models a more physically convincing origin.

We are currently extending the above developments in two ways. The first is that the motion of an elastically mounted rigid cylinder (mass: m_c) is allowed to have two degrees of freedom: in-line (x) and transverse (y), as illustrated in figure 11. The second extension is to model the structure as an elastic body, in particular, as an elastic beam. As such, the beam can be modelled to vibrate with bending in two planes as well as in extensional modes. Such a model would be more representative of an actual structure.

The use of the present method to derive the governing equations of more complicated fluid–structure interaction problems (e.g. the rigid cylinder can be replaced by a flexible rod) is something the authors feel would be a straightforward exercise. The limitations of the method are, in theory, only practical ones. The theory is well equipped to handle three-dimensional interactions, and body geometries of arbitrary shape. Of course, the mathematics necessary to obtain the governing equations becomes increasingly complex as the complexity of the problem increases. The simplification of the variational equations corresponding to these more complex problems is perhaps the biggest challenge.

In practice, the relevant field equations for a given fluid–structure interaction problem are often known *a priori*, and due to their complexity in even the simplest of cases, they are solved numerically. What is suggested is that the present framework is flexible. It is rich enough that it can be used to obtain equations needing computational solution, yet it is also simple enough in formulation to lead to reduced-order models.

This work is supported by the Office of Naval Research grant no. N00014-97-1-0017. We would like to thank our programme manager Dr Thomas Swean for his interest and financial support.

References

Adrezin, R., Bar-Avi, P. & Benaroya, H. 1996 Dynamic response of compliant offshore structures—review. *J. Aerosp. Eng.* **9**, 114–131. (doi:10.1061/(ASCE)0893-1321(1996)9:4(114))

Atsavapranee, P., Voorhees, A., Benaroya, H. & Wei, T. 1999 Lock-in regimes and vortex shedding modes on a cantilevered cylinder. In *ASCE Engineering Mechanics Division Conference, Baltimore, MD.*

Balasubramanian, S. & Skop, R. A. 1999 Vortex-excited dynamics of a tapered pivoted cylinder in uniform and shear flows. In *13th ASCE Engineering Mechanics Conference* (CD-ROM).

Barhoush, H., Namini, A. H. & Skop, R. A. 1995 Vortex shedding analysis by finite elements. *J. Sound Vib.* **184**, 111–127. (doi:10.1006/jsvi.1995.0307)

Batchelor, G. K. 1967 *An introduction to fluid dynamics.* New York, NY: Cambridge University Press.

Bearman, P. W. 1984 Vortex shedding from oscillating bluff bodies. *Annu. Rev. Fluid Mech.* **16**, 195–222. (doi:10.1146/annurev.fl.16.010184.001211)

Benaroya, H. & Wei, T. 2000 Hamilton's principle for external viscous fluid structure interaction. *J. Sound Vib.* **238**, 113–145. (doi:10.1006/jsvi.2000.3152)

Berger, E. & Wille, R. 1972 Periodic flow phenomena. *Annu. Rev. Fluid Mech.* **4**, 313–340. (doi:10.1146/annurev.fl.04.010172.001525)

Billah, K. Y. R. 1989 A study of vortex-induced vibration. PhD dissertation, Princeton University.

Birkhoff, G. & Zarantanello, E. H. 1957 *Jets, wakes, and cavities.* New York, NY: Academic Press.

Bishop, R. E. D. & Hassan, A. Y. 1964 The lift and drag forces on a circular cylinder oscillating in a flowing fluid. *Proc. R. Soc. A* **277**, 32–50. (doi:10.1098/rspa.1964.0004)

Cai, Y. & Chen, S. S. 1996 Dynamic response of a stack/cable system subjected to vortex induced vibration. *J. Sound Vib.* **196**, 337–349. (doi:10.1006/jsvi.1996.0487)

Chen, S. S., Zhu, S. & Cai, Y. 1995 An unsteady flow theory for vortex-induced vibration. *J. Sound Vib.* **184**, 73–92. (doi:10.1006/jsvi.1995.0305)

Christensen, C. F. & Ditlevsen, O. 1999 Random lock-in intervals for tubular structural elements subject to simulated wind. *J. Eng. Mech.* **125**, 1380–1389. (doi:10.1061/(ASCE)0733-9399(1999)125:12(1380))

Christensen, C. F. & Roberts, J. B. 1998 Parametric identification of vortex-induced vibration of a circular cylinder from measured data. *J. Sound Vib.* **211**, 617–636. (doi:10.1006/jsvi.1997.1393)

Currie, I. G. 2003 *Fundamental mechanics of fluids.* New York, NY: Marcel Dekker.

Dong, P. 2002 Phase averaged transport in the vortex-induced oscillation of a cylinder: experiment and modeling. PhD thesis, Rutgers University.

Dong, P., Benaroya, H. & Wei, T. 2004 Integrating experiments into an energy-based reduced-order model for vortex-induced-vibrations of a cylinder mounted as an inverted pendulum. *J. Sound Vib.* **276**, 45–63. (doi:10.1016/j.jsv.2003.07.041)

Dost, S. & Tabarrok, B. 1979 Application of Hamilton's principle to large deformation and flow problems. *J. Appl. Mech.* **46**, 285–290.

Facchinetti, M. L., de Langre, E. & Biolley, F. 2004 Coupling of structure and wake oscillators in vortex-induced vibrations. *J. Fluids Struct.* **19**, 123–140. (doi:10.1016/j.jfluidstructs.2003.12.004)

Fox, R. W. & McDonald, A. T. 1992 *Introduction to fluid mechanics*. New York, NY: Wiley.

Gabbai, R. D. & Benaroya, H. 2005 An overview of modeling and experiments of vortex-induced vibration of circular cylinders. *J. Sound Vib.* **282**, 575–616. (doi:10.1016/j.jsv.2004.04.017)

Goswami, I., Scanlan, R. H. & Jones, N. P. 1993*a* Vortex-induced vibration of circular cylinders. I: experimental data. *J. Eng. Mech.* **119**, 2270–2287. (doi:10.1061/(ASCE)0733-9399(1993)119:11(2270))

Goswami, I., Scanlan, R. H. & Jones, N. P. 1993*b* Vortex-induced vibration of circular cylinders. II: new model. *J. Eng. Mech.* **119**, 2288–2302. (doi:10.1061/(ASCE)0733-9399(1993)119:11(2288))

Grega, L., Wei, T., Leighton, R. & Neves, J. 1995 Turbulent mixed-boundary flow in a corner formed by a solid wall and a free surface. *J. Fluid Mech.* **294**, 17–46. (doi:10.1017/S0022112095002795)

Griffin, O. M. 1982 Vortex streets and patterns. *Mech. Eng.* March, 56–61.

Gupta, H., Sarkar, P. P. & Mehta, K. C. 1996 Identification of vortex-induced-response parameters in time domain. *J. Eng. Mech.* **122**, 1031–1037. (doi:10.1061/(ASCE)0733-9399(1996)122:11(1031))

Hartlen, R. T. & Currie, I. G. 1970 Lift-oscillator model of vortex-induced vibration. *J. Eng. Mech. Div.* **96**, 577–591.

Hover, F. S., Miller, S. N. & Triantafyllou, M. S. 1997 Vortex-induced vibration of marine cables: experiments using force feedback. *J. Fluids Struct.* **11**, 307–326. (doi:10.1006/jfls.1996.0079)

Hsu, T., Grega, L., Wei, T. & Leighton, R. 2000 Kinetic energy transport in a corner formed by a solid wall and a free surface. *J. Fluid Mech.* **410**, 343–366. (doi:10.1017/S0022112099008125)

Iwan, W. D. & Blevins, R. D. 1974 A model for vortex-induced oscillations of structures. *J. Appl. Mech.* **41**, 581–586.

Jadic, I., So, R. M. C. & Mignolet, M. P. 1998 Analysis of fluid–structure interactions using a time-marching technique. *J. Fluids Struct.* **12**, 631–654. (doi:10.1006/jfls.1998.0163)

Jordan, D. W. & Smith, P. 1994 *Nonlinear ordinary differential equations*. Oxford, UK: Oxford University Press.

Kim, Y. C. & Lee, P. M. 1990 Nonlinear motion characteristics of a long vertical cylinder. In *Proc. First Pacific/Asia Offshore Mechanics Symposium*, pp. 247–256.

King, R. 1977 A review of vortex shedding research and its application. *Ocean Eng.* **4**, 141–172. (doi:10.1016/0029-8018(77)90002-6)

Kitigawa, T., Fujino, Y. & Kimura, K. 1999 Effects of free-end condition on end-cell-induced vibration. *J. Fluids Struct.* **13**, 499–518. (doi:10.1006/jfls.1999.0214)

Krenk, S. & Nielsen, S. R. K. 1999 Energy balanced double oscillator model for vortex-induced vibrations. *J. Eng. Mech.* **125**, 263–271. (doi:10.1061/(ASCE)0733-9399(1999)125:3(263))

Leech, C. M. 1977 Hamilton's principle applied to fluid mechanics. *Q. J. Mech. Appl. Math.* **30**, 107–130. (doi:10.1093/qjmam/30.1.107)

Lin, J.-C. & Rockwell, D. 1999 Horizontal oscillations of a cylinder beneath a free surface: vortex formation and loading. *J. Fluid Mech.* **389**, 1–26. (doi:10.1017/S0022112099004747)

Lu, Q. S., To, C. W. S. & Jin, Z. S. 1996 Weak and strong interactions in vortex-induced resonant vibrations of cylindrical structures. *J. Sound Vib.* **190**, 791–820. (doi:10.1006/jsvi.1996.0094)

Malvern, L. E. 1969 *Introduction to the mechanics of a continuous medium*. Englewood Cliffs, NJ: Prentice Hall.

Marris, A. W. 1964 A review of vortex streets, periodic wakes, and induced vibration phenomena. *J. Basic Eng.* **86**, 185–196.

McIver, D. B. 1973 Hamilton's principle for systems of changing mass. *J. Eng. Mech.* **7**, 249–261. (doi:10.1007/BF01535286)

Nakagawa, K., Kishida, K. & Igarashi, K. 1998 Vortex-induced oscillation and lift of yawed cylinders in cross-flow. *J. Fluids Struct.* **12**, 759–777. (doi:10.1006/jfls.1998.0157)

Noca, F. 1997 On the evaluation of time-dependent fluid-dynamic forces on bluff bodies. PhD thesis, California Institute of Technology.

Sarpkaya, T. 1979 Vortex induced oscillations: a selective review. *J. Appl. Mech.* **46**, 241–258.

Sarpkaya, T. 1995 Hydrodynamic damping, flow-induced oscillations, and biharmonic response. *ASME J. Offshore Mech. Arct. Eng.* **117**, 232–238.

Sarpkaya, T. 2004 A critical review of the intrinsic nature of vortex-induced vibrations. *J. Fluids Struct.* **19**, 389–447. (doi:10.1016/j.jfluidstructs.2004.02.005)

Shah, P., Atsavapranee, P., Hsu, T., Wei, T. & McHugh, J. 1999 Turbulent transport in the core of a trailing delta wing vortex. *J. Fluid Mech.* **387**, 151–175. (doi:10.1017/S0022112099004553)

Shah, P., Atsavapranee, P., Wei, T. & McHugh, J. 2000 The role of turbulent elongational stresses on deflocculation in paper sheet formation. *TAPPI J.* **83**, 70.

Sibetheros, I. A., Miskad, R. W., Ventre, A.-V. & Lambrakos, K. F. 1994 Flow mapping of the reversing vortex wake of a cylinder in planar harmonic flow. In *Proc. Fourth Int. Offshore and Polar Engineering Conference,* pp. 406–412.

Skop, R. A. & Balasubramanian, S. 1995*a* A nonlinear oscillator model for vortex shedding from a forced cylinder. Part 1: uniform flow and model parameters. In *Proc. Fifth Int. Offshore and Polar Engineering Conference*, pp. 578–581.

Skop, R. A. & Balasubramanian, S. 1995*b* A nonlinear oscillator model for vortex shedding from a forced cylinder. Part 2: shear flow and axial diffusion. In *Proc. Fifth Int. Offshore and Polar Engineering Conference*, pp. 582–586.

Skop, R. A. & Balasubramanian, S. 1997 A new twist on an old model for vortex-excited vibrations. *J. Fluids Struct.* **11**, 395–412. (doi:10.1006/jfls.1997.0085)

Skop, R. A. & Griffin, R. A. 1973 A model for the vortex-excited resonant response of bluff cylinders. *J. Sound Vib.* **27**, 225–233. (doi:10.1016/0022-460X(73)90063-1)

Smith, G. 1992 Turbulent cascade to small scales during the off-axis collision of two vortex rings. Master's thesis, Rutgers University.

Ventre, A.-V. 1993 Flow vizualization of a planar oscillatory flow around a cylinder. Master's thesis, University of Texas at Austin.

Vikestad, K., Vandiver, J. K. & Larsen, C. M. 2000 Added mass and oscillatory frequency for a circular cylinder subjected to vortex-induced vibrations and external disturbance. *J. Fluids Struct.* **14**, 1071–1088. (doi:10.1006/jfls.2000.0308)

Williamson, C. H. K. & Govardhan, R. 2004 Vortex-induced vibrations. *Annu. Rev. Fluid Mech.* **36**, 413–455. (doi:10.1146/annurev.fluid.36.050802.122128)

Xing, J. T. & Price, W. G. 1997 Variational principles of nonlinear dynamical fluid–solid interaction systems. *Phil. Trans. R. Soc. A* **355**, 1063–1095. (doi:10.1098/rsta.1997.0053)

Zdrakovich, M. M. 1996 Different modes of vortex shedding: an overview. *J. Fluids Struct.* **10**, 427–437. (doi:10.1006/jfls.1996.0029)

Zhou, C. Y., So, R. M. C. & Lam, K. 1999 Vortex-induced vibrations of an elastic circular cylinder. *J. Fluids Struct.* **13**, 165–189. (doi:10.1006/jfls.1998.0195)